

Towards net-zero emissions through the hybrid SMR-solar cogeneration plant equipped with modular PCM storage system for seawater desalination



Khashayar Sadeghi^{a,*}, Seyed Hadi Ghazaie^a, Riccardo Chebac^b, Ekaterina Sokolova^a, Evgeniy Fedorovich^a, Antonio Cammi^b, Marco Enrico Ricotti^b, Amir Saeed Shirani^c

^a Peter the Great St. Petersburg Polytechnic University, Department of Nuclear and Heat Power Engineering, 195251 Saint Petersburg, Russian Federation

^b Department of Energy, Nuclear Engineering Division, Politecnico di Milano, Via La Masa 34, 20156 Milan, Italy

^c Shahid Beheshti University of Iran, Faculty of Nuclear Engineering, P.O. Box: 1983963113, Tehran, Iran

HIGHLIGHTS

- The effects of using the rejected water of NPP's condenser as the feedwater of the desalination plan
- Developing three different schemes based on SMR-Solar cogeneration plant equipped with modular PCM storage system
- Developing a new program based on the Fortran language to simulate various components of the schemes
- A general techno-economic comparison of SMR-Solar cogeneration schemes for desalination

ARTICLE INFO

Keywords:

Seawater desalination
Hybrid nuclear-renewable
Cogeneration plant
PCM storage system
Small modular reactor

ABSTRACT

In the existing nuclear power plants, almost 60 to 70% of produced heat in the reactor is released to the ambient through the condenser, which can be used as the feedwater of reverse osmosis (RO) desalination plants. Although increasing the temperature of RO feedwater improves the overall performance, the quality of produced water decreases. This difficulty can be solved by blending the high-quality water produced by thermal desalination plants (DPs) with RO products. However, supplying the required energy for driving the thermal DP needs to consume a huge amount of fossil fuel, which is contrary to net zero-emission goals. In this study, three different scenarios, based on the solar plant (SP) (scenario 1), small modular reactor (SMR) (scenario 2), and the hybrid SMR-SP (scenario 3) for supplying the required energy of DP have been suggested. According to the techno-economic evaluation conducted in this study, using the SMR as the auxiliary heat source of the SP in the third scenario can be considered as a promising technology, which is associated with several benefits. However, the average water cost in scenario 2 is 66 (cent/m^3), which is almost 8.5 and 5% less than scenarios 1 and 3, respectively.

1. Introduction

The Sustainable Development Goals (SDGs), which were set in September 2015 by world leaders, include 17 goals to end poverty, prosperity, and growth for all human beings. One of the most important of these goals was water management since the planet's biodiversity and water resources are under pressure and environmental change is exacerbating the world's water problem [1]. Currently, using modern seawater desalination technologies for producing freshwater has been considered as the best solution to water shortage in many countries.

Technically, the seawater desalination process is formed of five essential components including two inputs (feed water and energy), two outputs (fresh water and rejected water), and the core element (seawater desalination technology). Seawater desalination is a chemical-mechanical process, in which a huge amount of energy should be consumed [2]. During last decades, the main energy sources for driving the large-scale desalination plants (DPs) mostly were fossil-fuel-based power plants. However, the significant drawbacks of these sources such as CO₂ emission and finite resources of fossil fuel have generated considerable interest in terms of using sustainable energy resources among

* Corresponding author.

E-mail address: sadegi.h@edu.spbstu.ru (K. Sadeghi).

governments [3]. Among all the available sustainable and renewable energy resources, solar and nuclear energy are known as the best alternative options to traditional energy resources for driving large-scale DPs [4,5]. Potentially, both solar and nuclear power plants can provide two main required energy forms (heat and electricity) for DPs. The form of required energy in the desalination process depends on the type of desalination technology (heat, electricity, or both of them). Generally, desalination methods can be classified into three groups, namely, evaporation-condensation, filtration, and crystallization [6–8]. The most well-known desalination technologies, which have the capability of producing thousands of cubic meters of freshwater during day and night, are multi-effect distillation (MED), multi-stage flash desalination (MSF), and reverse osmosis (RO). One of the main technical differences between thermal desalination technologies (MED and MSF) and RO is the quality of produced freshwater [9–11]. The thermal technologies can treat very salty water (with the quality of 30,000 to 70,000 ppm) and produce pure water with quality of less than 25 ppm, while the quality of produced water by RO system depends on many factors such as temperature and salinity of feed water. The average total dissolved solids (TDS) of the final product in large-scale RO desalination systems is almost 300 to 400 mg/l [11–13]. One of the main common techniques to increase the performance of RO desalination and consequently, decrease the total cost of water produced is pre-heating the feed water of the RO unit [5,14]. The average temperature of RO feed water depends on the average temperature of seawater. Increasing the average seawater temperature to a higher value needs to consume energy and usually, designers prefer to use the waste energy of power plants to perform the pre-heating process. The released energy from the turbine condenser of nuclear power plants (NPPs) is one of the best sources of waste energy. The average temperate of rejected (hot stream) of the NPP's condenser water in the normal operation of NPP is more than 34 °C (as an instance for a pressurized water reactor (PWR)). On the other hand, the amount of intake water in NPP's condenser is often enough to supply the feed water of a large-scale DP (for a PWR-1000 MW_e NPP this value is about 4.5 to 7.5×10^6 m³/day) [15,16]. Hence, it can be highly recommended to consume this heated-water as the feed water of RO system. This integration between NPP and water plant leads to numerous advantages such as increase the recovery ratio of membranes, decrease the power consumption in DP, decrease the consumed energy for driving the water plant, and consequently, decrease the energy cost and decreasing the capital cost of DP due to removing the intake-out take water infrastructure from DP (the intake-out take pipelines of NPP can be used for both plants) [5].

However, using the rejected water of the NPP's condenser as the RO feed water is not always a positive approach and it can include some drawbacks. It can be proved that increasing the temperature of membrane feed water leads to an increase in total dissolved solid (TDS) of produced water [17]. One of the pre-eminent methods to decrease the TDS of produced water by RO system in large-scale DPs is using hybrid desalination technologies. Due to the fact that the quality of produced water by thermal technologies is much better than RO, blending the produced water from two technologies with various qualities can lead to a more acceptable overall quality. For supplying the required heat for thermal DPs, which are installed close to an NPP to use the rejected water of the condenser as feed water, steam extraction from the turbine of NPP can be considered as an appropriate solution. In arid regions, usually, the average annual solar irradiance can provide a special opportunity to install a solar power plant (SPP) equipped with thermal storage system (TSS) to afford enough heat for driving a large-scale thermal DP. However, both these power generation sources have some drawbacks such as safety risk and electricity demand during the day (for NPP) and the absence of solar energy at nights (for SPP). Hence, it can be proposed a hybrid power generation unit, which is an integration of both NPP and SPP to cover weak points of each other.

There is a vast amount of literature on using solar or nuclear power plants to drive a large-scale DP. In [5] the authors investigated the

possible hybrid desalination schemes integrated with the nuclear power plant. According to the obtained results of this study using the hot stream of the NPP's condenser for DP feedwater is considered the best hybrid option. Recently, the authors in [18] have performed a feasibility study of solar-nuclear hybrid system for distributed power source. According to the findings of this study, hybrid system shows better performance in terms of capacity factor than the solar plant. However, to the authors, very few publications can be found in the literature that discusses the issues of analyzing large-scale hybrid DPs powered by NPP and SPP equipped with phase change material storage system (PCMSS), especially the integration of all these combinations in one unique unit. Most of the previous works do not take into account the hybrid power generation unit (nuclear and solar) with hybrid desalination systems. In this paper, while the authors refer to their earlier works [5,19–22], the focus is different. The main goal of this study is a general techno-economic comparison of using standalone NPP and SPP equipped with PCMSS and a combination of them to supply the required heat of thermal DP in order to improve the quality of produced water by RO system, which is fed by hot stream of the NPP's condenser.

The remainder of this paper is structured as follows. In **Section 2** (problem statement section) the effect of feed water temperature on the quality of produced water by RO system is analyzed. **Section 3** outlines the general explanation of various proposed schemes, mathematical formulations for implementing the parabolic-trough SPP and phase changed material storage system, and a simulation of Advanced Lead Fast Reactor European Demonstrator (ALFRED). In this section, a new computer code for techno-economic evaluation of each configuration is developed. In **Section 4**, the obtained results of each configuration for a certain case study are presented, and finally, in **Section 5** a brief conclusion is given.

2. Temperature effects on the quality of produced water in reverse osmosis desalination system; problem statement

Recently, the role of RO desalination system in the global water market has been expanded due to the unrivaled properties such as low specific energy consumption (SEC). RO system utilizes only electricity to produce freshwater. Numerous parameters have impacts on the energy consumption of RO system. However, the effect of feedwater temperature (T_f) is completely obvious. The ascending variation of T_f in a logical range of 15 to 40 °C leads to a decrease in water viscosity, which consequently leads to an increase in membrane permeability and flux permeation. By increasing the membrane permeability not only recovery ratio of the system and overall performance increase but also the energy consumption of high pressure pump of the system decreases. These effects can be appeared in the temperature-dependence formula of recovery ratio and permeate flux change through the membrane, which is given by [23]:

$$RR = 1 - \frac{0.00115}{P_{max}} \times TDS \times \left(\left(\frac{\mu(25^\circ\text{C})}{\mu(T_f^\circ\text{C})} \right) \right) \times \left(\frac{T_f^\circ\text{C} + 273.15}{25 + 273.15} \right) \quad (1)$$

$$\varphi_t = \frac{\text{Membrane permeability at temperature } T_f^\circ\text{C}}{\text{Membrane permeability at temperature } 25^\circ\text{C}} = e^{K \times \left(\left(\frac{1}{273 + T_f^\circ\text{C}} \right) - \left(\frac{1}{273 + 25^\circ\text{C}} \right) \right)} \quad (2)$$

where, RR is the recovery ratio, P_{max} is the maximum design pressure of the membrane (bar), μ is the dynamic viscosity (N · S/m²), K is the constant characteristic for the membrane material, and φ_t is temperature correction factor. It should be noted that temperature 25 °C in **formulas (1) and (2)** is considered as the reference point, in which the permeate flux through membrane is equal to one.

Despite the fact the feedwater temperature rise has a positive effect on SEC of RO system, the negative points of this process also should be considered. It can be proved that the most serious negative consequence

of feedwater temperature rise is the increase in the TDS of produced fresh water. This principle can be formulated by the following term:

$$TDS_{out} = \left(\frac{TDS_{feed} \times \dot{m}_{nom}}{800 \times \dot{m}_{des}} \right) \times \left(1 + \frac{1}{1 - RR} \right) \times (1 + (T_f - 25) \times 0.03) \quad (3)$$

where, TDS_{out} and TDS_{feed} are the quality of produced water and feedwater of RO method, respectively, \dot{m}_{nom} is nominal permeate flux ($\text{l/m}^2\text{h}$), and \dot{m}_{des} is the design average permeate flux ($\text{l/m}^2\text{h}$). To realize the effects of feedwater temperature on the quality of RO production clearly, a theoretical test has been conducted. The properties of RO setup are listed in Table 1. In this test, the calculations are performed in the range of 25 to 40 °C. The results obtained from the preliminary analysis of feedwater effects on RO system operational parameters show that using the rejected water of NPP's condenser is an effective way to increase the performance and decrease the required energy [17,23].

According to [24], the TDS of standard drinking water should not exceed more than 300 ppm. With regard to formula (3), TDS of produced water increases by feedwater temperature rise. In Fig. 1, the counter plot of TDS with respect to operational parameters has been shown. The most striking result to emerge from this figure is that at the temperature of 36 °C and recovery ratio of more than almost 32%, the TDS of water exceeds more than the standard value (300 ppm). It must be stressed that according to formula (1), the corresponded recovery ratio with feedwater temperature of 36 °C is equal to 37%, which is in the non-standard region in Fig. 1. As it was explained in Section 1, one of the best ways to improve the water produced quality is blending RO production with freshwater purified by the thermal desalination methods. The key point in this process is estimating the required freshwater produced by the thermal unit, which should be added to RO production. This evaluation can be performed using the hybridization degree. This parameter can be expressed as the ratio of the water produced by thermal DP to the total water production (RO + thermal). In this study, the criterion for selecting the hybridization degree is improving the water quality.

The required hybridization degree for producing standard water can be obtained by:

$$H_d = \frac{W_{th}}{W_{RO} + W_{th}} \quad (4)$$

$$TDS_{tot} = \frac{(TDS_{out} \times W_{RO}) + (TDS_{th} \times W_{th})}{W_{RO} + W_{th}} \quad (5)$$

where, H_d is hybridization degree, W_{RO} and W_{th} are capacity of RO and thermal desalination units, TDS_{th} is the water quality of thermal DP, and TDS_{tot} is the final quality of water.

Fig. 2 indicates four significant factors including hybridization degree, capacity of RO and MED plants, feedwater temperature, and TDS of produced water at various temperatures. The left vertical axis in this figure indicates the minimum hybridization degrees for producing freshwater with acceptable TDS (equal to or less than 300 ppm) based on the feedwater temperatures. As an example, the required H_d at the temperature of 36 °C (which is equal to the temperature of rejected water from typical NPP's condenser, operating at normal conditions) is

Table 1
The technical properties of RO system.

Parameter	Value
$\dot{m}_{feedwater}$ (kg/s)	694
P_{max} (bar)	69
$\dot{m}_{des}, \dot{m}_{nom}$ ($\text{l/m}^2\text{h}$)	14, 28
K	3500
W_{RO} (m^3/day)	20,000
$TDS_{feed}, TDS_{tot}, TDS_{th}$ (ppm)	43,000, 300, 25

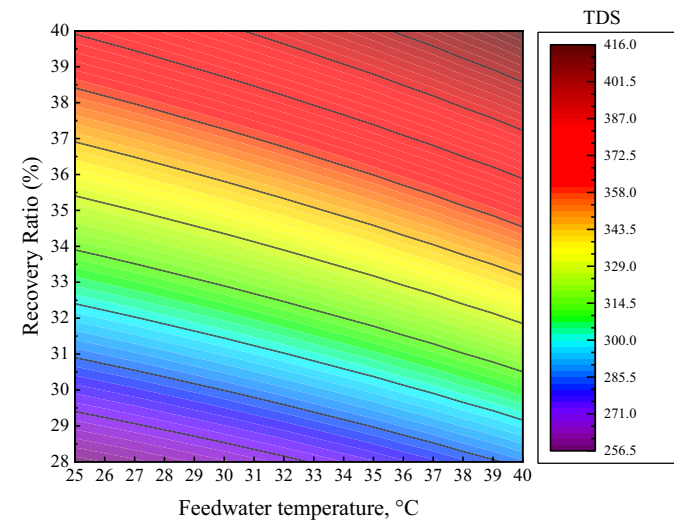


Fig. 1. Counter plot of total dissolved solids based on changing the feedwater temperature and recovery ratio.

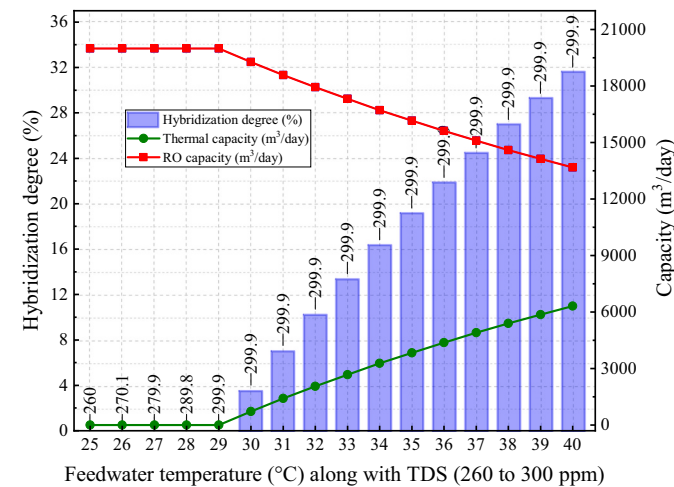


Fig. 2. Calculated H_d to produce water with standard TDS and the capacity of thermal and RO desalination units depending on feedwater temperature.

22%, which determines that for a total capacity of 20,000 (m^3/day), the shares of RO and thermals unit are 15,620 and 4380 (m^3/day), respectively.

This section has reviewed the positive and negative effects of feedwater temperature rise on SEC and TDS and it has been proved that the hybrid DP can be used as a reliable method for improving the TDS. In the next section, several scenarios for supplying the required energy for driving the thermal DP will be given.

3. Power generation systems for driving the thermal DP

This section has been divided into three parts. In the first part, after a brief overview of solar DP and various types of storage systems, the algorithm for the combination of TSS, SPP, and DP is given. The next part provides a new module for ALFRED simulation coupled with DP. Finally, in the last part of Section 3, the new approach for the combination of SPP, NPP, TSS, and DP has been presented.

3.1. First scenario: thermal DP powered by parabolic trough SPP equipped with TSS

In this study, the proposed scheme for solar DP is based on the MED unit, which is powered by parabolic troughs solar concentrators. Despite the outstanding features of solar DP such as no pollution and global warming effects and no fuel cost, this technology suffers from a major drawback of climate-related variability. In order to reduce or eliminate the intermittency effects of solar radiation, deploying storage systems is widely suggested by designers. PCM-based storage systems with distinguished properties such as acceptable phase change temperature and thermal conductivity for many applications, high density, negligible volume change, and proper half-time of the crystallization rate have made massive progress in energy storage technology [25]. The first step of designing PCMSS is the material selection, which is based on the application of PCMSS. In this work, the main focus is placed on driving the MED desalination system with a required steam temperature of 70 °C. Therefore, the suggested PCM for calculations is RT100 (paraffine) with melting point of 100 (°C).

3.1.1. Mathematical modeling of the first scenario

The general scheme of the first configuration for producing freshwater is presented in Fig. 3. As can be seen in this scheme, the heat transfer fluid (HTF) in collectors absorbs the maximum possible energy from solar radiation. The absorbed energy is transferred to PCMSS through the intermediate heat exchanger, in which the mass flow rate and interest temperature can be set. MED desalination unit is connected to PCMSS to receive the required energy for producing steam in the first effect. In order to model the integrated system, all the main components such as solar field, intermediate heat exchanger, PCMSS, and MED unit numerically should be simulated. Practically, the solar field (SF) is formed of several loops of solar collector assemblies including a number of parabolic collectors and their receivers. In this study, to reduce the complexity of calculations, SF is assumed to be a single node and consequently, absorber energy, losses, temperature, pressure drop, and other performance parameters can be calculated for a single node, independent of each solar collector assemblies.

3.1.1.1. Energy balance of single node SF. In order to determine the temperature rise across SF, a well-known energy balance equation in steady-state can be implemented as:

$$\Delta T_{SF} = \frac{\dot{Q}_{abs}}{\dot{m}_{HTF} C_{HTF}} \rightarrow T_{SF,out} = \frac{\dot{Q}_{abs}}{\dot{m}_{HTF} C_{HTF}} + T_{SF,in} \quad (6)$$

where, \dot{Q}_{abs} is the energy absorption rate in SF (kW), ΔT_{SF} is the temperature rise across SF, \dot{m}_{HTF} is the mass flow rate of HTF ($\frac{\text{kg}}{\text{s}}$), C_{HTF} is the heat capacity of HTF ($\frac{\text{kJ}}{\text{kg°C}}$), and $T_{SF,in}$ and $T_{SF,out}$ are input and output temperatures of HTF to SF (°C), respectively.

However, due to the thermal inertia related to the energy state of the single node, which highly impacts the performance of the system, a steady-state model is not sufficient. Thermal mass (TM) of HTF in the receivers and also in the piping system of SF, which leads to absorb and store heat energy in the node, is considered as the most important transient term, which should be added to the energy balance equation. According to Fig. 4, the energy balance of SF, including the net absorption and net loss energy, can be rewritten as:

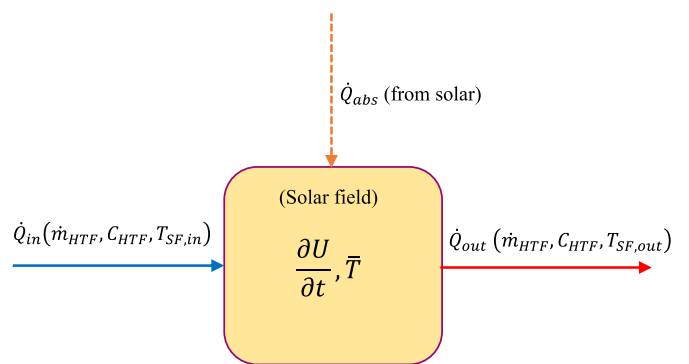


Fig. 4. Energy balance of single node SF: The control volume, including the HTF within the absorber tubes and piping for single node SF.

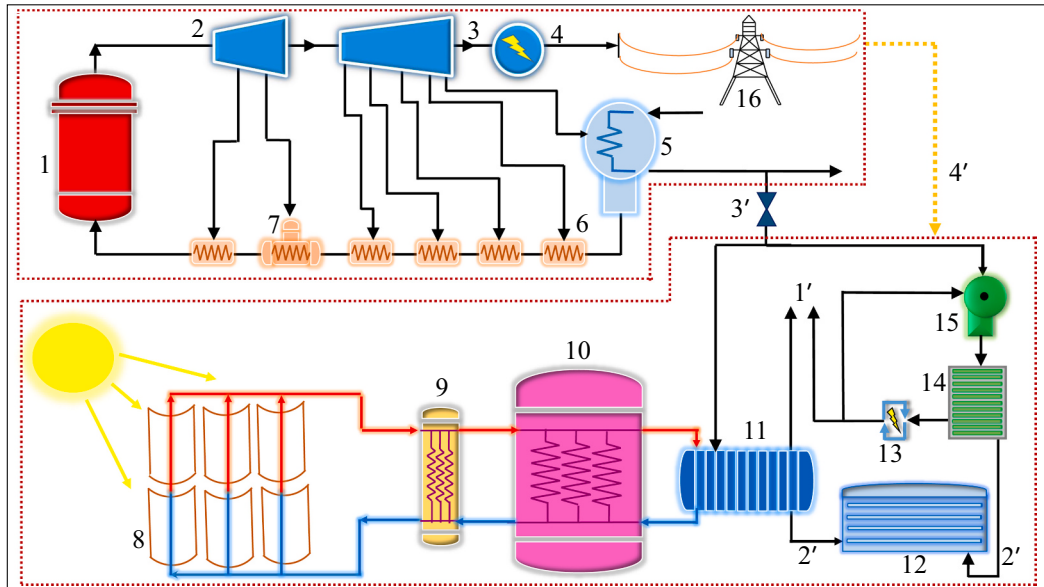


Fig. 3. The general scheme of the first scenario (ALFRED-based NPP, SPP + PCMSS, DP): 1 – ALFRED, 2 – high-pressure turbine, 3 – low-pressure turbine, 4 – generator, 5 – condenser of the NPP, 6 – preheater, 7 – deaerator, 8 – solar field, 9 – intermediate heat exchanger, 10 – PCMSS, 11 – thermal DP, 12 – water storage tank, 13 – energy recovery unit of RO plant, 14 – membrane modules, 15 – high-pressure pump, 16 – grid, 1' – rejected brine pipeline, 2' – produced freshwater pipeline, 3' – hot stream of the NPP's condenser as the feed water for DP, 4' – electricity to DP from NPP.

$$\frac{\partial U}{\partial t} = \dot{Q}_{in,SF} - \dot{Q}_{out,SF} + \dot{Q}_{abs,SF}, \quad (7)$$

where

$$\dot{Q}_{in,SF} - \dot{Q}_{out,SF} = \dot{m}_{HTF} C_{HTF} (T_{SF,in} - T_{SF,out}), \quad (8)$$

and $\dot{Q}_{in,SF}$ and $\dot{Q}_{out,SF}$ are the energy rates of input and output HTF to SF.

On the other hand, the internal energy term $\left(\frac{\partial U}{\partial t}\right)$ based on the temperature changes can be represented as:

$$\frac{\partial U}{\partial t} = (m_{HTF} C_{HTF} + m_{TM} L_{piping}) \frac{\partial T}{\partial t}, \quad m_{HTF} = \rho_{HTF} L_{piping} A_{piping}, \quad (9)$$

where $m_{TM} L_{piping}$ dimensionally is equal to the $m_{HTF} C_{HTF}$ term and is composed of total thermal mass (m_{TM} (kg)) and total length of piping (L_{piping} (m)), A_{piping} is the total area of piping (m^2), ρ_{HTF} is the density of HTF, and m_{HTF} is the total mass of HTF (kg).

By defining the \bar{T} as the average temperature single node inlet and outlet, and substituting in Eqs. (8) and (9), the result is:

$$\frac{\partial \bar{T}}{\partial t} = \frac{2\dot{m}_{HTF}(T_{SF,in} - \bar{T}) + \dot{Q}_{abs,SF}}{(m_{HTF} C_{HTF} + m_{TM} L_{piping})}, \quad \bar{T} = \frac{(T_{SF,in} - T_{SF,out})}{2}, \quad (10)$$

The solution of linear first-order Eq. (10) using initial condition of $\bar{T} = \bar{T}_0$ at $t = 0$ can be written as:

$$T_{SF,out} = T_{SF,in} + \frac{\dot{Q}_{abs,SF}}{\dot{m}_{HTF} C_{HTF}} + 2 \left(\bar{T}_0 - T_{SF,in} - \frac{\dot{Q}_{abs,SF}}{2\dot{m}_{HTF} C_{HTF}} \right) e^{\frac{-2\dot{m}_{HTF} \Delta t}{m_{HTF} C_{HTF} + m_{TM} L_{piping}}} \quad (11)$$

where Δt as the time interval depends on the time-step of the solar radiation dataset.

In this work, \dot{Q}_{abs} is obtained using system Advisor Model program (SAM), which is a powerful software in simulating renewable-based power generation, particularly SPP, and is developed by the National Renewable Energy Laboratory (NREL) [26,27]. Despite the fact that SAM is a robust software, PCMSS modeling has not been configured in this program.

3.1.1.2. Mathematical modeling of PCMSS. The developed thermal model for PCMSS in this work is based on a simplified method for modeling the thermal performance of the storage system with a well-mixed configuration (mixture of HTF and PCM), where the overall temperature of PCMSS is a constant value in each time step [28]. It is also assumed that the phase change process is isothermal and the heat transfer between HTF and PCM takes place directly. Similar to solar field modeling, energy balance equations for PCMSS also can be written as follow:

$$\frac{\partial U}{\partial t} = \dot{Q}_{0,PCMSS} + \dot{Q}_{in,PCMSS} - \dot{Q}_{out,PCMSS} - \dot{Q}_{lost,PCMSS}, \quad (12)$$

$$\frac{\partial U}{\partial t} = (m_{HTF} C_{HTF} + m_{pcm} C_{pcm}) \frac{\partial T}{\partial t}, \quad (13)$$

$$\dot{Q}_{in,PCMSS} = \dot{m}_{HTF} C_{HTF} (T_{in,pcm} - T_{pcm}), \quad (14)$$

$$\dot{Q}_{out,PCMSS} = \dot{m}_{HTF} C_{HTF} (T_{pcm} - T_{out,pcm}), \quad (15)$$

$$\dot{Q}_{lost,PCMSS} = UA(T_{pcm} - T_{amb}), \quad (16)$$

where $\dot{Q}_{0,PCMSS}$ is the remaining heat in the system, $\dot{Q}_{in,PCMSS}$ and $\dot{Q}_{out,PCMSS}$ is the energy rate of the charge and discharge of PCMSS (kW), respectively, $\dot{Q}_{lost,PCMSS}$ is the lost power from PCMSS (kW), $T_{in,pcm}$ and $T_{out,pcm}$ are the input and output temperatures of PCMSS ($^{\circ}\text{C}$),

respectively, T_{amb} is the ambient temperature, T_{pcm} is the average temperature of the PCM ($^{\circ}\text{C}$), U is the overall heat transfer coefficient of the PCMSS ($\frac{\text{kW}}{\text{m}^2 \cdot ^{\circ}\text{C}}$) and A is the heat transfer area m^2 .

By substituting Eqs. (14) to (16) in Eq. (12) and applying some simplification on Eq. (13) one can write:

$$Q_{PCMSS}(t) = Q_{PCMSS}(t - \Delta t) + \dot{m}_{HTF} C_{HTF} (T_{in} - T_{pcm}) - \dot{m}_{HTF} C_{HTF} (T_{pcm} - T_{out}) - UA(T_{pcm} - T_{amb}), \quad (17)$$

where $Q_{PCMSS}(t)$ is the stored energy in PCMSS at time-step t . The maximum temperature that HTF can have in SF can be called the set temperature (T_{set}), which depends on the HTF type and its thermodynamic properties as well as the pipe material. The program performs the calculations with an initial value for HTF mass flow rate. Then the output temperature of SF should be compared with the set temperature. If this value is more than the set temperature, then the new mass flow rate should be calculated by Eq. (18):

$$\dot{m}_{HTF} = \frac{\dot{Q}_{abs,PCMSS}(t) \times 1000}{C_{HTF} (T_{set} - T_{SF,in})} \quad (18)$$

However, sometimes the available solar radiation is so high. Accordingly, to keep the outlet temperature of SF under the set temperature, the mass flow rate should be increased dramatically, which is not possible for any pump. Therefore, a limitation for the mass flow rate of HTF should be specified and in the case of exceeding the calculated mass flow rate from this set point, solar collectors should be defocused, and a part.

The energy range of PCMSS, in which PCM is in two-phase region (solid-liquid), has a minimum and maximum limitations and can be calculated using the properties of the PCMSS material.

$$Q_{min} = \varphi_{pcm} V_{TSS} \rho_{pcm} C_{pcm} T_{pcm}, \quad (19)$$

$$Q_{max} = Q_{min} + \varphi_{pcm} V_{TSS} \rho_{pcm} h_{pcm,phase\ change}, \quad (20)$$

$$\varphi_{pcm} = \frac{V_{PCM}}{\sum V_{PCM}, V_{HTF}}, \quad V_{TSS} = \frac{M_{pcm}}{\rho_{pcm} \varphi_{pcm}}, \quad M_{pcm} \\ = \frac{\text{Capacity (MWh)} \times 3.6 \times 10^6}{h_{pcm,phase\ change}}, \quad (21)$$

where, φ_{pcm} is the PCM fraction, V_{PCM} and V_{HTF} are the volumes of PCM and HTF respectively (m^3), M_{pcm} is the total mass of PCM (kg) and $h_{pcm,phase\ change}$ is the heat of fusion ($\frac{\text{kJ}}{\text{kg}}$).

During the PCM melting process, the PCM-fraction (f) indicates the liquid portion per total amount of PCM. This parameter, which varies from 0 to 1, depends on the stored energy in each time-step and can be obtained by

$$\begin{cases} \text{If } Q_{PCMSS}(t) < Q_{min} \text{ then } f = 0 \\ \text{If } Q_{min} < Q_{PCMSS}(t) < Q_{max} \text{ then } f = \frac{Q_{PCMSS}(t) - Q_{min}}{Q_{max} - Q_{min}}, \\ \text{If } Q_{PCMSS}(t) > Q_{max} \text{ then } f = 1 \end{cases} \quad (22)$$

and finally, according to the Eq. (13) and the definition of f , PCM average temperature in single-phase region (solid or liquid) and two-phase state can be gained by

$$\begin{cases} \text{If } (f=0 \text{ or } f=1) \text{ then } T_{pcm}(t - \Delta t) = \frac{Q_{PCMSS}(t) - Q_{PCMSS}(t - \Delta t)}{(m_{HTF} C_{HTF} + m_{pcm} C_{pcm})} + T_{pcm}(t - \Delta t), \\ \text{If } (0 < f < 1) \text{ then } T_{pcm}(t - \Delta t) \end{cases} \quad (23)$$

3.1.1.3. Intermediate loop performance model based on the effectiveness-NTU method. Installing an intermediate heat exchanger between SF and PCMSS can regularize the input temperature to the storage system as well as prevent any contact between HTFs of SF and PCMSS. The absorbed solar energy can be transferred to PCMSS directly, only in the case that HTFs of both sides are the same. It should be noted that even if the material of HTFs of both sides are the same, the intermediate heat exchanger would be a useful component since in some cases the pressure of HTF in SF is different from other parts. For example, in this study, pressurized water is used as the HTF in SF to prevent any evaporation at high temperatures. However, the pressure of water for charging the PCMSS is not necessary to be high and to reduce material costs and increase safety aspects. Hence, by determining a proper mass flow rate, all the possible energy from the solar field can be recovered at a normal temperature. The Number of Transfer Units (ε -NTU) method as a proper technic for outlet fluid temperature prediction in heat exchangers for a counter-flow arrangement can be implemented. This method is based upon a dimensionless parameter, which is called heat transfer effectiveness, and can be formulated as (Fig. 5):

$$\varepsilon = \frac{\text{actual heat transfer rate}}{\text{maximum possible heat transfer rate}} = \frac{\dot{Q}_{\text{actual}}}{\dot{Q}_{\text{max}}}, \quad (24)$$

where

$$\dot{Q}_{\text{actual}} = (\dot{m}C)_{\text{hot}}(T_{\text{hot,in}} - T_{\text{hot,out}}) = (\dot{m}C)_{\text{cold}}(T_{\text{cold,out}} - T_{\text{cold,in}}), \quad (25)$$

$$\dot{Q}_{\text{actual}} = (\dot{m}C)_{\text{min}}(T_{\text{hot,in}} - T_{\text{cold,out,t}}),$$

$$\text{and } \begin{cases} \text{If } \dot{m}C_{\text{hot}} < \dot{m}C_{\text{hot}} \text{ then } (\dot{m}C)_{\text{min}} = \dot{m}C_{\text{hot}}, (\dot{m}C)_{\text{max}} = \dot{m}C_{\text{cold}} \\ \text{If } \dot{m}C_{\text{cold}} < \dot{m}C_{\text{hot}} \text{ then } (\dot{m}C)_{\text{min}} = \dot{m}C_{\text{cold}}, (\dot{m}C)_{\text{max}} = \dot{m}C_{\text{hot}} \end{cases}, \quad (26)$$

where ε is the effectiveness of IL, $T_{\text{hot,in}}$ and $T_{\text{hot,out}}$ are input and output temperatures of the hot stream to IL ($^{\circ}\text{C}$), respectively, and $T_{\text{cold,out}}$ and $T_{\text{cold,in}}$ are input and output temperatures of the cold stream of IL ($^{\circ}\text{C}$), respectively.

The NTU, which expresses the non-dimensional size of the heat exchanger, can be given in terms of ε based on the semi-empirical formula depending on heat exchanger configuration. Eq. (28) suggests a convenient formula for the counter-flow heat exchanger arrangement:

$$\text{NTU} = \frac{\log\left(\frac{1-\varepsilon C_R}{1-\varepsilon}\right)}{1-C_R} \text{ where } C_R = \frac{(\dot{m}C)_{\text{min}}}{(\dot{m}C)_{\text{max}}}, \quad (28)$$

The total surface area in the heat exchanger can be estimated using

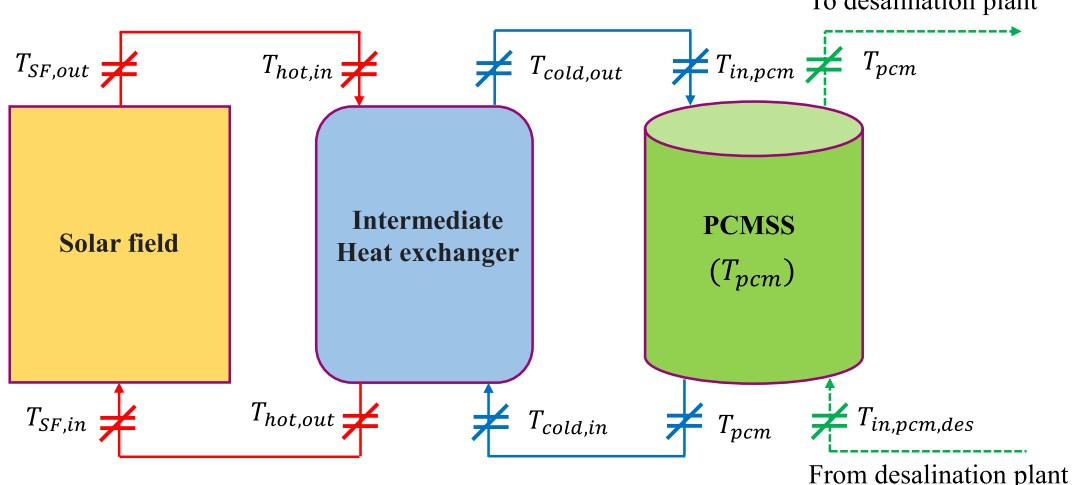


Fig. 5. Schematic diagram of solar thermal power generation system for driving the DP.

the overall heat transfer coefficient U and NTU:

$$A = \frac{\text{NTU } (\dot{m}C)_{\text{min}}}{U}, \quad (29)$$

Other important findings from the ε -NTU method are output temperatures in each time-step, which can be obtained by some algebraic simplifications on mentioned formulas [29]:

$$\begin{aligned} T_{\text{cold,out}}(t+1) &= \frac{1}{C_R} \times [T_{\text{cold,in}}(t) \times (C_R - \varepsilon)] + (\varepsilon \times T_{\text{hot,in}}(t)), \\ T_{\text{hot,out}}(t+1) &= \frac{1}{C_R} \times [T_{\text{hot,in}}(t) \times (C_R - \varepsilon)] + (\varepsilon \times T_{\text{cold,in}}(t)), \end{aligned} \quad (30)$$

3.1.1.4. Simulation modeling of MED desalination unit. In this section, a general simulation for MED plant based on thermodynamic input parameters and technical conditions is developed. The consumed power in MED unit is the main unknown parameter, which should be obtained. This parameter depends on the total plant capacity and gain output ratio (GOR) of MED unit. Following this, the total required heat can be obtained as [5]:

$$\dot{Q}_{\text{desalination}} \text{ (MW)} = \frac{\text{GOR} \times W_{\text{th}} \times h_{\text{latent}}}{24 \times 3600}, \quad (31)$$

In formula (31), h_{latent} is known as the latent heat of vaporization, which depends on temperature and pressure, which can be found by [30]:

$$h_{\text{latent}} = 2501.897149 - 2.407064037 \times T_{\text{hex,MED}} + 1.192217 \times 10^{-3} \times (T_{\text{hex,MED}})^2 - 1.5863 \times 10^{-5} \times (T_{\text{hex,MED}})^3, \quad (32)$$

where

$$T_{\text{hex,MED}} = T_{\text{mb}} + T_{\text{hex,drop}} + \Delta T_{\text{steam,max brine}}, \quad (33)$$

In formula (33), the average temperature drop in MED stages ($T_{\text{hex,drop}}$) and temperature difference between feed steam and maximum brine temperature ($\Delta T_{\text{steam,max brine}}$) are given to the program by the user. GOR depends on MED effects (NE) and is given by:

$$\text{GOR} = 0.8 \times \text{NE}, \quad (34)$$

where

$$\text{NE} = \text{Integer} \left(\frac{T_{\text{ope,MED}} \text{ (Overall operating temperature of MED)}}{T_{\text{drop,effects}} \text{ (Average temperature drop between effects)}} \right),$$

And

To desalination plant

T_{pcm}

T_{pcm}

From desalination plant

$$T_{ope,MED} = T_{mb} - T_{cw} - T_{cr}, \quad (35)$$

In formula (35), the user should initialize both cooling water temperature (T_{cw}) and MED condenser range ($T_{ope, MED}$) before running the program [31,32].

3.1.1.5. The economic evaluation of the first scenario. According to the problem statement in Section 2, the final product is produced water from a hybrid system including RO and MED plants. In this paper, it is assumed that the total specific cost of produced water by RO system can be obtained using the program of Techno-Economic Analysis of Nuclear Desalination (TEAND), which is developed in [5] and is linked to the developed program of this work. The required electrical energy in the suggested scheme is assumed to be supplied by NPP, located next to SPP. On the other hand, the entire required heat energy for driving thermal DP should be provided by SPP. Therefore, it is necessary to evaluate the Levelized cost of heat cost (LCOH) of both SPP and NPP. In Table 2, the economic evaluation formulation for LCOH of parabolic-trough heat system, including solar field, PCMSS, intermediate heat exchanger, and other auxiliary equipment, is given. The economic evaluation of LCOH for selected NPP will be described in Section 3.2.2.

Table 2

The key economic formulas used to estimate the leveled cost of heat of SF [33–37]

Formula	Description
$Cost_{cons, PCMSS}^{Spe} = Cost_{PCM}^{Spe} + Cost_{Tank}^{Spe} + Cost_{Insu}^{Spe} + Cost_{Found}^{Spe}$	$Cost_{cons, PCMSS}^{Spe}$: specific construction cost of PCMSS $(\frac{\$}{kWh_t})$
$Cost_{Insu}^{Spe}$	$Cost_{PCM}^{Spe}$: cost of PCM $(\frac{\$}{kWh_t})$
$Cost_{Tank}^{Spe}$	$Cost_{Tank}^{Spe}$: cost of PCM tank $(\frac{\$}{kWh_t})$
$Cost_{Insu}^{Spe}$	$Cost_{Insu}^{Spe}$: cost of insulation $(\frac{\$}{kWh_t})$
$Cost_{Found}^{Spe}$	$Cost_{Found}^{Spe}$: foundation cost $(\frac{\$}{kWh_t})$
$Cost_{overnight} = ((Cost_{cons, SF}^{Spe} + Cost_{IL}^{Spe}) \times Power_{SP}) + (Cost_{cons, PCMSS}^{Spe} \times Capacity_{PCMSS})$	$Cost_{overnight}^{Spe}$: overnight construction cost (\$)
$IDC_{SP} = ((1 + ir)^{\left(\frac{Le}{24}\right)} - 1) \times Cost_{overnight}$	$Cost_{cons, SF}^{Spe}$: specific construction cost of SF $(\frac{\$}{kWh_t})$
$TPI_{SP} = IDC_{SP} + Cost_{overnight}$	$Cost_{IL}^{Spe}$: specific construction cost of SF $(\frac{\$}{kWh_t})$
$CRF_{SP} = \frac{DR \times (1 + DR)^{LSP}}{(1 + DR)^{LSP-1}}$	$Power_{SP}$: nominal output power of SP (kW)
$Cost_{Annual, capital, SP} = TPI_{SP} \times CRF_{SP}$	$Capacity_{PCMSS}$: nominal capacity of PCMSS (kWh _t)
$Cost_{Annual, OM, SP} = 0.15 \times Cost_{Annual, capital}$	IDC_{SP} : interest during construction of SP
$Cost_{Annual, other, SP} = 0.1 \times Cost_{Annual, capital}$	ir : interest rate (%)
$Cost_{Annual, total, SP} = Cost_{Annual, capital, SP} + Cost_{Annual, OM, SP} + Cost_{Annual, other, SP}$	Le : construction duration of SP (month)
$LCOH_{SP} = \frac{Cost_{Annual, total}}{E_{Annual}}$	TPI_{SP} : total plant investment (\$)
	CRF_{SP} : capital recovery factor
	DR : discount rate (%)
	LSP : lifetime of SP (year)
	$Cost_{Annual, capital, SP}$: annualised capital cost of SP (\$)
	$Cost_{Annual, OM, SP}$: annual operating and maintenance cost of SP (\$)
	$Cost_{Annual, other, SP}$: annual other costs of SP (\$)
	$Cost_{Annual, total, SP}$: annual total costs of SP (\$)
	$LCOH_{SP}$: leveled cost of heat of SF (\$/(kWh _t))
	E_{Annual} : annual net energy produced (kWh _t)

After estimating the $LCOH_{SP}$, the total cost of produced water by thermal DP can be obtained. In Table 3, the economic evaluation formulation for the water plant is stated.

Fig. 6 presents a well-established algorithm, corresponded to the calculation procedure for the first configuration, in order to provide a deeper understanding of using the mentioned formulas.

3.2. Second scenario: ALFRED as the heat source of thermal DP

Currently, new Generation IV nuclear systems, which not only can generate electricity with higher efficiency, but also can be used as a part of the co-generation systems, are developing. In this work, a model of the Advanced Lead Fast Reactor European Design (ALFRED) has been considered for developing a co-generation system to supply the required energy of a thermal DP. ALFRED is a 300 MW_{th} pool-type system with removable components. The main design parameters of ALFRED have been listed in Table 4.

The proposed secondary cycle of ALFRED is formed of two turbine configurations, which are connected to the generator. In Fig. 7, the general scheme of ALFRED-based cogeneration for producing freshwater has been demonstrated. The produced electricity of NPP drives the RO system, while the extracted steam supplies the required heat of thermal DP.

3.2.1. Dymola ALFRED simulator

The simulation of ALFRED-based NPP has been carried out by means of an object-oriented approach, implemented into Dymola software based on the well-documented Modelica language. The full description of the Dymola has been given in previous works of authors [38–41]. In this program, both steady-state and transient analysis of the ALFRED-based NPP can be performed. As a result of the extreme flexibility of the program, the required steam for driving the thermal DP can be extracted at any desired pressure from turbine configuration. In Fig. 8,

Table 3

The key economic formulas used to estimate the total cost of produced water [5,21,31,32]

Formula	Description
$Cost_{cons, DP} = 1.2 \times W_{th} \times Cost_{base, DP}$	$Cost_{cons, DP}$: total construction cost (\$)
$IDC_{DP} = ((1 + ir)^{\left(\frac{Ld}{24}\right)} - 1) \times Cost_{cons, DP}$	$Cost_{base, DP}$: total specific base cost of DP (\$/m ³ /day)
$TPI_{DP} = IDC_{DP} + Cost_{cons, DP}$	IDC_{PCMSS} : interest during construction (\$)
$CRF_{DP} = \frac{DR \times (1 + DR)^{LWP}}{(1 + DR)^{LWP-1}}$	Ld : construction duration of DP (month)
$Cost_{Annual, capital, DP} = TPI_{DP} \times CRF_{DP}$	TPI_{DP} : total plant investment (\$)
$Cost_{Annual, heat, DP} = \dot{Q}_{desalination} \times LPC_{SP} \times 8760 \times \alpha_{DP} \times 10^3$	CRF_{WP} : capital recovery factor
$Cost_{Annual, ele, DP} = \left[\frac{1.5 + 0.1(GOR - 10) \times W_{th}}{24 \times 10^3} \right] \times LPC_{SP} \times 8760 \times \alpha_{DP} \times 10^3$	DR : discount rate (%)
$Cost_{Annual, OM, DP} = 0.3 \times Cost_{Annual, capital, DP}$	LWP : lifetime of WP (year)
$Cost_{Annual, total, DP} = Cost_{Annual, capital, DP} + Cost_{Annual, heat, DP} + Cost_{Annual, ele, DP} + Cost_{Annual, OM, DP}$	$Cost_{Annual, capital, DP}$: annualised capital cost of DP (\$)
$Cost_{water} = \frac{Cost_{Annual, total, DP}}{W_{th} \times 365 \times \alpha_{ava}}$	$Cost_{Annual, heat, DP}$: annual heat cost of DP (\$)
	α_{DP} : combined SP/DP load factor (%)
	$Cost_{Annual, ele, DP}$: annual electrical cost of DP (\$)
	$Cost_{Annual, OM, DP}$: annual operating and maintenance cost of DP (\$)
	$Cost_{Annual, total, DP}$: total annual cost of DP (\$)
	$Cost_{water}$: total cost of produced water $(\frac{\$}{m^3})$
	α_{ava} : water production availability (%)

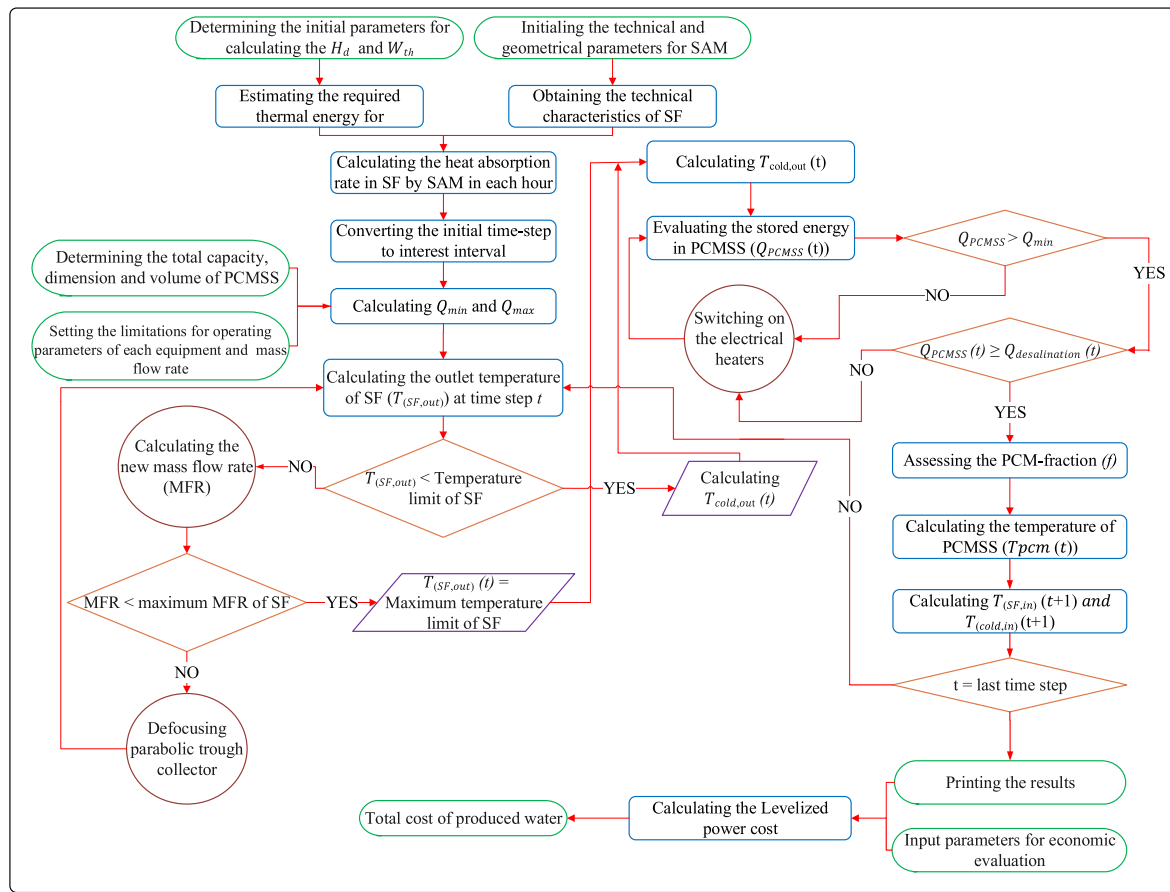


Fig. 6. Comprehensive algorithm of calculations for the first scenario.

Table 4
main design parameters of ALFRED.

Parameter	Value	Unit
Thermal power	300	MW _{th}
Thermal efficiency	41.6	%
Coolant mass flow rate	25,984	kg/s
Number of fuel assemblies	171	–
Coolant inlet temperature	400	°C
Coolant outlet temperature	480	°C
Number of steam generator and primary pump	8	–
Steam generator feedwater inlet temperature	335	°C
Steam generator feedwater outlet temperature	450	°C
Live steam pressure	180	bar

the Dymola turbine model group with extraction valve is demonstrated.

3.2.2. Economic assessment of the second scenario

In this section, a model for evaluating the LPC of ALFRED-based NPP is provided. The key factor in estimating the LCOE is the specific construction cost (\$/kWh_t) of NPP. According to the scaling law, which has been presented in [42], the specific construction cost of ALFRED-based NPP should be estimated based on a reference NPP and four technical factors, namely learning factor (α_L), modularity factor (α_{MD}), multiple units factor (α_{MU}), and design factor (α_{DF}).

$$cost_{s,c,ALFRED} = cost_{s,c,reference} \times \left(\frac{power_{ALFRED}}{power_{reference}} \right)^{(n-1)} \quad (36)$$

where $cost_{s,c,ALFRED}$ and $cost_{s,c,reference}$ are the specific construction cost of ALFRED-based NPP and reference NPP, respectively, and n can be ranged from 0.4 to 0.7 [43]. The main role of four technical factors is

implementing the benefits of SMR design to the unit base cost of the NPP. Hence, the obtained $cost_{s,c,ALFRED}$ should be multiplied by four technical factor parameters (α):

$$\alpha = \alpha_L \times \alpha_{MD} \times \alpha_{MU} \times \alpha_{DF} \quad (37)$$

The learning factor depends on the number of similar NPPs constructed both in the country and worldwide. According to [42], this factor can be ranged from 65% to 100% for maximum 20 reactor units on the same site. The separate fabrication of various SMR components leads to a reduction in the capital cost of the plant. As an instance, the value of α_{MD} for ALFRED is 85%. In [42], a general diagram has been demonstrated to estimate this factor for all types of SMRs. By sharing the fixed cost of the site among the multiple units on the same site, a cost reduction will appear. The suitable range related to this factor (α_{MU}) decreases from 100% to almost 65% by increasing the number of reactor units on the same site [42]. Finally, the design factor can be defined as a cost reduction by any possible design simplification for SMRs. According to [42], α_{DF} is 10% for 350–150 MWe plants. It should be mentioned that, in this paper, the specific construction cost of reference NPP (1100 MWe) is 3200 €/kWh_t. By estimating the $cost_{s,c,ALFRED}$ based on the formula (36), LCOE can be obtained using the listed formulas in Table 5: ([5,32]):

3.3. Third scenario: ALFRED-based NPP equipped with PCMSS as the auxiliary heat source of SPP

The main role of the electrical heater in PCMSS is supplying the required energy of DP during windy or cloudy days. It should be noted that the operation of the water plant should not be stopped to avoid any reduction in the overall performance of the system. However, converting the generated electricity to heat energy through auxiliary electrical heaters in PCMSS is not recommended. On the other hand, using the

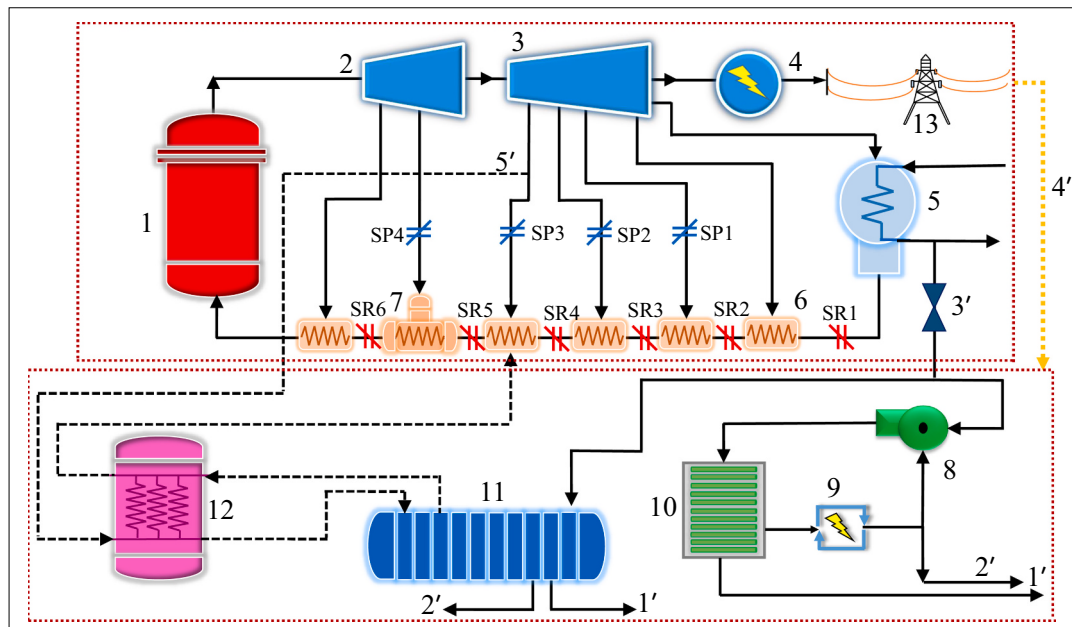


Fig. 7. The general scheme of second scenario (ALFRED as the heat source of thermal DP): 1 – reactor building, 2 – high-pressure turbine, 3 – low-pressure turbine, 4 – generator, 5 – condenser of the NPP, 6 – preheater, 7 – deaerator, 8 – high-pressure pump, 9 – energy recovery unit of RO plant, 10 – membrane modules, 11 – thermal DP, 12 – intermediate heat exchanger, 13 – grid, 1' – produced freshwater pipeline, 2' – rejected brine pipeline, 3' – hot stream of the NPP's condenser as the feed water for DP, 4' – electricity to DP from NPP. 5' – extracted steam from turbine, SP1 to SP4 – possible points for steam extraction, SR1 to SR6 – possible points for steam return.

diesel auxiliary power unit leads to carbon dioxide emission in the site, which is contrary to the net-zero emission goals. Extracted steam from turbine configuration of NPP as the auxiliary power unit of thermal DP can be counted as a reliable, sustainable, and clean heat source. In this scheme, the energy of extracted steam at an appropriate pressure and temperature should be accumulated in a PCMSS, which is located close to the second cycle of ALFRED. In this case, PCMSS can play the role of the intermediate loop to increase the safety of the co-generation plant. In Fig. 9 the general scheme of the third scenario is illustrated. The required electricity of RO and MED plants can be supplied from NPP's generator. Similar to the previous scenarios, the required feedwater of all desalination units is provided by the hot stream of the NPP's condenser. The economic evaluation of this scheme is formed of three sections including NPP, SPP + PCMSS, and DP cost estimation. The necessary formulas and methodology for both technical and economic assessment of this scheme are given in previous sections.

4. Results and discussion

Among all the possible regions, authors have selected United Arab Emirates (UAE) as the case study since this country is located in the Southwest of Asia with significant solar radiation and also increasing demand for fresh water in arid regions. In 2009, the UAE government signed a contract with the state-run utility firm Korea Electric Power Corporation (KEPCO) to construct four APR-1400 NPP units at the Barakah site by 2020. Regarding the location of the Barakah site, the area near this site can be selected as an appropriate place for a combination of NPP, SPP, and DP. In this section, the comprehensive techno-economic analysis of each scenario is performed and finally, a general comparison between obtained results will be taken place to select the most optimum option.

4.1. Techno-economic evaluation of the first scenario

As the first step, some important parameters of climate conditions related to the selected region are presented. The demonstrated data in

Fig. 10 are generated based on the 2020 data library. The main climatic parameters used in SAM software are listed in Table 6. The selected time intervals of this study are the first three days of two months, namely January and July.

In this study, water has been selected as HTF since the DP plant in this study (MED) is a low-temperature technology and the required temperature for driving MED is less than 100 °C (almost 70 °C in this work). Hence, water is the best option for HTF to reduce the material, operating, and maintenance costs. The amount of power leaving in HTF depends on the area of the solar field and the required energy for thermal DP. As it was mentioned in Section 2, the total capacity of the designed desalination plant is 20,000 m³/day, in which the minimum hybridization degree for producing freshwater with acceptable TDS is 22%. The total required heat for 4400 m³/day produced water by MED plant should be calculated using formula (31). In Table 7, the values of necessary parameters for calculating the required heat and also designed parameters related to Fig. 5 are listed. With respect to these values, the total required heat is 10.6 MWe.

The target solar multiple should be determined before performing further calculations. According to [44], the solar multiple of 2.5 leads to a suitable value of TSS effectiveness. In Fig. 11, the thermal power $\dot{Q}_{abs,SF}$ incident on the receiver in SF is demonstrated. The average amount of received thermal power in hot month is almost 55% more than the cold month.

The maximum allowable output temperature of solar field ($T_{SF,out}$) is set to 140 °C. By considering this limitation, to transfer all the possible absorbed heat in the solar field, the mass flow rate of HTF should be changed in each step and the maximum allowable mass flow rate of HTF should be determined before calculations.

On the other hand, it has been assumed that the PCMSS operates in the two-phase state. During the operation of the plant, the PCMSS will start the work at the set-point temperature (ambient temperature) in the solid region. The stored sensible heat in the solid region will not be used in discharge mode since the purpose of designing this system is to use the latent heat in PCM. According to Fig. 11, the amount of received heat in the solar field is not the same in various months. Hence, in the case that

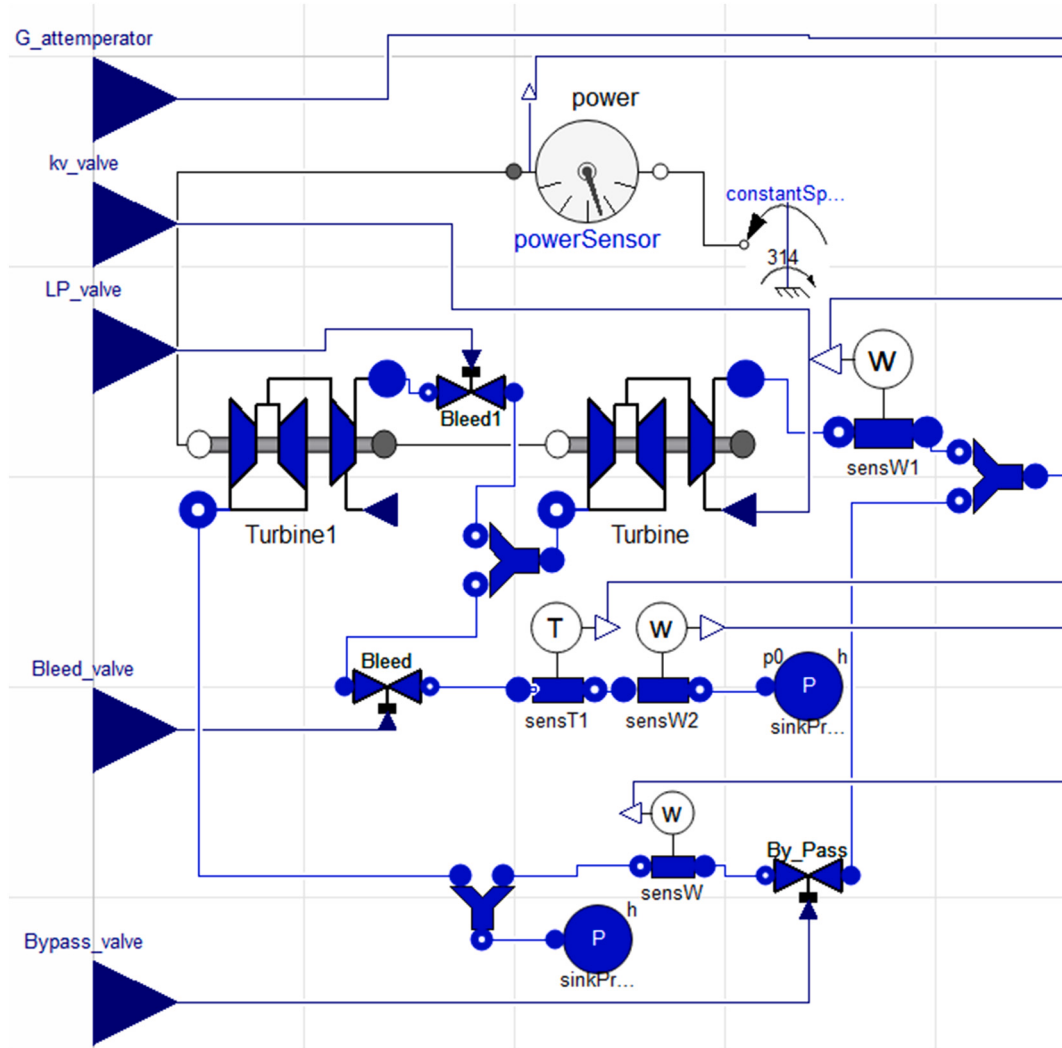


Fig. 8. Dymola turbine model group with extraction valve; G_Attemperator: attemperator mass flow rate, kv_valve: Turbine admission valve coefficient, LP_valve: low-pressure stage admission valve, bleed_valve: the valve that opens for steam extraction.

the PCMSS is designed based on the hot month, the capacity of the system is very large and consequently, during the cold month, most of the received heat will be stored in the sensible phase. One of the best solutions to this difficulty is dividing the main PCMSS into several smaller modules and some of these modules will be activated depending on the received heat in each month. Therefore, determining the optimum number of PCMSS modules and their capacities should be carried out. The other important point that should be noticed is the part of the required energy of thermal DP, which can be supplied by SPP. Solar fraction, which is defined as the supplied energy of DP from SPP per total supplied energy by heater and SPP, can be used as a suitable indicator to express the performance of the entire system. The capacity of the designed PCMSS should not be very large that decreases the solar fraction and also should not be very small that forces the collectors to refuse an amount of available solar radiation (solar field defocusing losses). With that being said, a general optimization on PCMSS based on the maximum mass flow rate of the solar field, the capacity of PCMSS, number of PCMSS modules, solar fraction, and the solar field defocusing losses should be performed. In Fig. 12, the solar fraction of the designed system depending on various maximum HTF mass flow rates and different PCMSS capacities is demonstrated. According to this picture, the maximum solar fraction of the system in the cold month (29%) can be obtained by a 7 MWh PCMSS. If the PCMSS capacity gets less than this value, a part of the useful energy should be rejected. On the flip side, a

capacity higher than 7 MWh leads to an increase in sensible capacity. The best solar fraction for the hot month is about 62%, which is obtained based on seven PSMSS modules of 7 MWh (49 MWh totally). Fig. 13 also suggests the proper maximum HTF mass flow rate corresponding to the highest solar fraction. The obtained results show that maximum HTF mass flow rates higher than 300 and 150 (kg/s) for the hot and cold months, respectively, lead to the highest solar fractions.

In Fig. 13, the solar waste heat versus a continuous range of PCMSS capacity based on various maximum HTF mass flow rates is presented. It can be seen from the data in this figure that the minimum capacity corresponded to the minimum solar waste heat is 49 and 7 MWh for hot and cold months, respectively. Any increase in the obtained capacities only leads to an increase in the capital cost of the system without any significant positive effect on the performance of the system.

In Fig. 14 the amount of consumed solar and auxiliary energy for driving the thermal DP is presented. The overall required energy for thermal DP is 2.75 TJ, of which 0.803 TJ and 1.717 TJ are supplied by solar energy in cold and hot months, respectively.

In Fig. 15, the total stored energy in PCMSS during each second is presented. It has been assumed that the initial temperature of the PCMSS is equal to the ambient temperature and consequently, the initial energy in PCMSS is zero. By increasing the temperature of PCMSS the stored energy also increases until it reaches the minimum required energy for phase changing (9.169×10^7 kJ for the hot month and 1.31×10^7 kJ for

Table 5

The key economic formulas used to estimate the LPC of ALFRED based nuclear power plant.

Formula	Description
$Cost_{overnight} = cost_{s. c., ALFRED} \times (1 + \alpha_{add} + \alpha_{con})$	$Cost_{overnight}$: overnight construction cost (\$) α_{add} : additional site-related construction cost factor α_{con} : NPP contingency factor
$IDC_{NPP} = \left((1 + ir) \left(\frac{Le}{24} \right) - 1 \right) \times Cost_{overnight}$	IDC_{NPP} : interest during construction of NPP ir : interest rate (%) Le : construction duration of NPP (month)
$TPI_{NPP} = IDC_{NPP} + Cost_{overnight}$	TPI_{NPP} : total plant investment (\$)
$CRF_{NPP} = \frac{DR \times (1 + DR)^{LNP}}{(1 + DR)^{LNPP} - 1}$	CRF_{NPP} : capital recovery factor DR : discount rate (%) $LNPP$: lifetime of NPP (year)
$Cost_{Annual, capital, NPP} = TPI_{NPP} \times CRF_{NPP}$	$Cost_{Annual, capital, NPP}$: annualised capital cost of NPP (\$)
$Cost_{Annual, OM, NPP} = 0.15 \times Cost_{Annual, capital}$	$Cost_{Annual, OM, NPP}$: annual operating and maintenance cost of NPP (\$)
$Cost_{Annual, other, NPP} = 0.1 \times Cost_{Annual, capital}$	$Cost_{Annual, other, NPP}$: annual other costs of NPP (\$)
$Cost_{Annual, total, NPP} = Cost_{Annual, capital, NPP} + Cost_{Annual, OM, NPP} + Cost_{Annual, other, NPP}$	$Cost_{Annual, total, NPP}$: annual total costs of NPP (\$)
$LCOE_{NPP} = \frac{Cost_{Annual, total}}{E_{Annual}}$	$LCOE_{NPP}$: LCOE of NPP (\$/(kWh _e)) E_{Annual} : annual net energy produced (kWh _e)

the cold month). After this point, the surplus solar energy will be saved in the PCM and at the same time, the liquid fraction also increases. It should be noted that increasing the capacity of PCMSS leads to storing the entire surplus energy in the solid-liquid region. However, based on the results of Fig. 12, an increase in the PCMSS capacity leads to a reduction in solar fraction and overall system performance. It is important to bear in mind that the HTF of DP only utilizes the latent heat of PCMSS and due to this, the level of stored energy after the first charge never drops to less than 105% of the minimum required energy for phase change (the extra 5% should be stored in the system to avoid any

solidification of PCM during the operation).

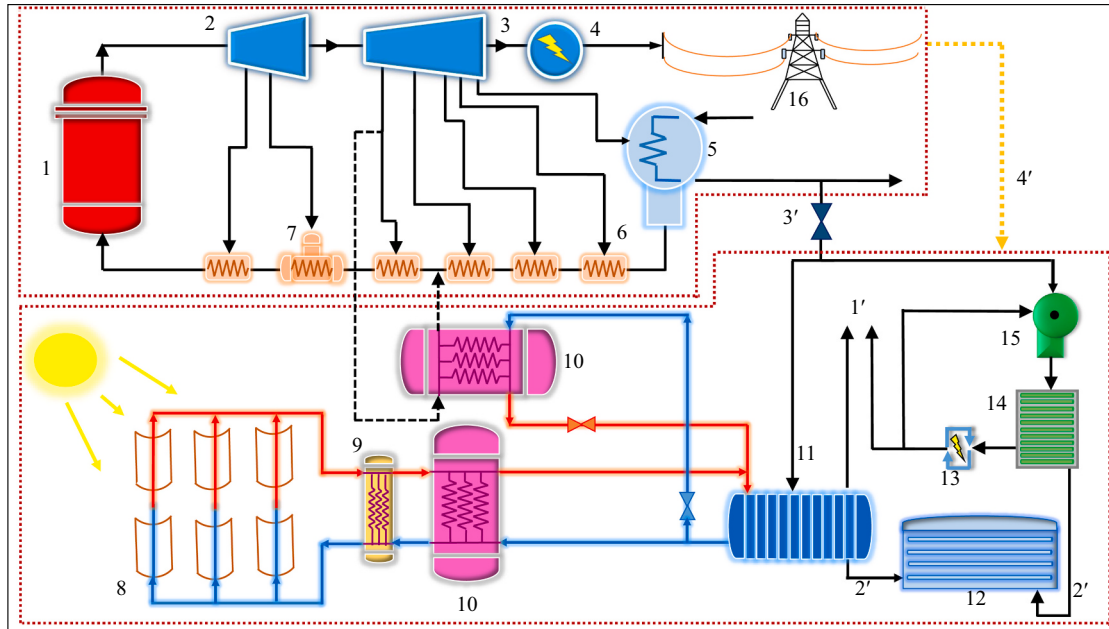
The total cost of produced water ($Cost_{total, hybrid}$) is a combination of produced water cost from thermal DP ($Cost_{th}$) and RO plant ($Cost_{RO}$), which can be evaluated by:

$$Cost_{total, hybrid} \left(\frac{\$}{m^3} \right) = \frac{(Cost_{th} \times W_{th}) + (Cost_{RO} \times W_{RO})}{W_{RO} + W_{th}} \quad (38)$$

the cost of the produced water from RO plant has been calculated using the developed procedure in [5], which is equal to $0.64 \left(\frac{\$}{m^3} \right)$. The LCOE of ALFRED-based NPP is evaluated by the given algorithm in Table 5. The input economic parameters for the LCOE calculation have been listed in Table 8. The obtained LCOE for ALFRED-based NPP is 8.3 $\left(\frac{\text{cent}}{\text{kWh}_e} \right)$, which can be used as the energy cost for driving RO plant, electrical auxiliary heater, and other electrical equipment and instruments in the system. The leveled cost of generated energy in the SPP is not constant and can vary day by day since a part of the total energy is generated by the auxiliary heater, which uses nuclear electricity. Formula (38) gives the total LPC of generated energy in SPP (LPC_{SPP}^{total}):

$$\begin{aligned} &LCOH_{SPP}^{total} \left(\frac{\text{cent}}{\text{kWh}_t} \right), \\ &= \frac{(LCOE_{NPP} \times \text{Total auxiliary energy}) + (LCOH_{SF} \times \text{Total solar energy})}{(\text{Total auxiliary energy} + \text{Total solar energy})} \end{aligned} \quad (39)$$

where, $LCOH_{SF}$ is the cost of generated heat by solar field. It has commonly been assumed that the efficiency of the electrical heater is 100% and consequently, the electrical and heat leveled cost for the auxiliary heater is the same. By applying the illustrated procedure for $LCOH_{SPP}^{total}$ calculation in Table 2 and using the given input parameters in Table 9, $LCOH_{SPP}^{total}$ can be obtained, which equals $4.06 \left(\frac{\text{cent}}{\text{kWh}_t} \right)$. Table 10 compares the amount of consumed energy from different energy sources. As can be seen, the average value of for $LCOH_{SPP}^{total}$ in the hot month is 21% higher than the cold month.



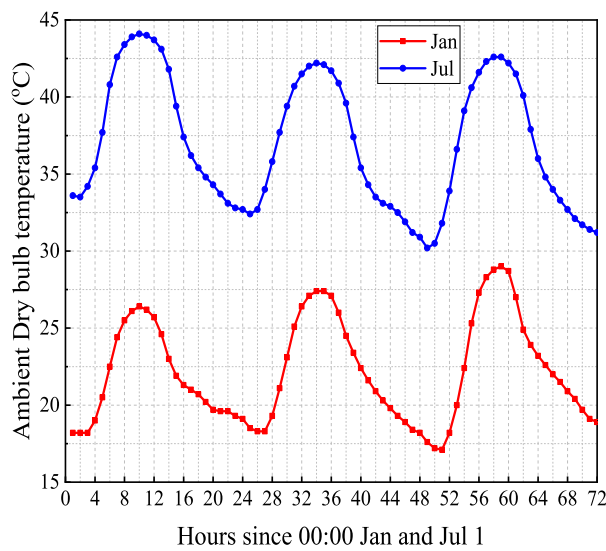


Fig. 10. Ambient temperature and beam nominal irradiance of the selected region during first three days of two months.

Table 6
Initial input parameters of SAM.

Parameter	Value	Parameter	Value
Latitude (DD)	23.97	Direct normal (beam) (kWh/m ² /day)	4.6
Longitude (DD)	52.22	Diffuse horizontal (kWh/m ² /day)	2.34
Elevation (m)	3	Average temperature (°C)	29
Global horizontal (kWh/m ² /day)	5.52	Average wind speed (m/s)	3.2

Table 7
Input parameters for calculating the required heat of thermal DP and designed parameters related to Fig. 5

Parameter	Value	Parameter	Value
$T_{drop, effects}$ (°C)	2.5	T_{cw} (°C)	25
T_{mb} (°C)	70	T_{cr} (°C)	10
$T_{hex, drop}$ (°C)	2.5	$\Delta T_{steam, max brine}$ (°C)	0.5
$T_{SF, out}, T_{hot, in}$ (°C)	140	GOR	11
$T_{SF, in}, T_{hot, out}$ (°C)	120	$T_{cold, out}, T_{in, pcm}$ (°C)	110
$T_{in, pcm, des}$ (°C)	80	$T_{cold, in}, T_{pcm}$ (°C)	100

The cost of produced water by thermal DP can be calculated using Table 3. In Table 12, the details of the energy costs in thermal DP are listed. According to Table 11, the average total energy cost of DP in hot months 18% is less than the cold month. The total costs of produced water for both RO and MED units are shown in Table 12. As can be observed in this table, the total water cost of the hybrid plant, which is obtained using formula (38), during the hot month is 2.5% less than the cold month.

Fig. 16 shows the portions of different cost components for thermal DP during two months.

4.2. Techno-economic evaluation of the second scenario

In this section, the Dymola ALFRED simulator has been used to model the second cycle of NPP. Table 13 provides various technical parameters of some significant points in ALFRED-based NPP. From this table, it can be concluded that steam temperature and pressure of live steam are higher than DP requirements. On the other hand, the mass flow rate of low-pressure pre-heater is not enough to supply the required energy. Power loss factor, which is defined as the loss of electrical power

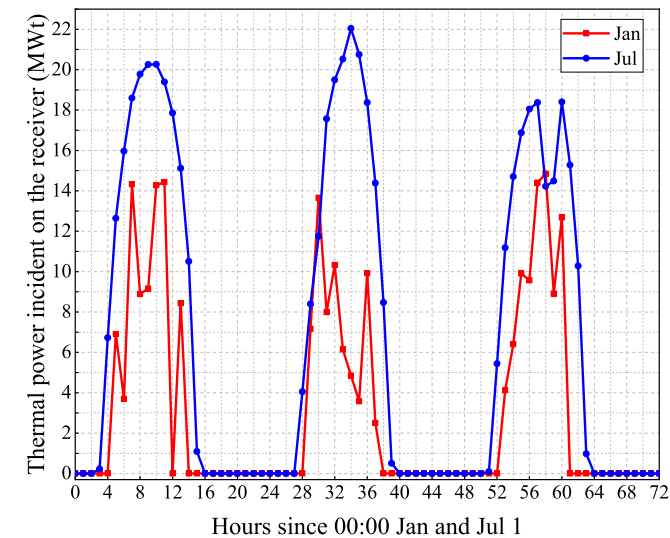
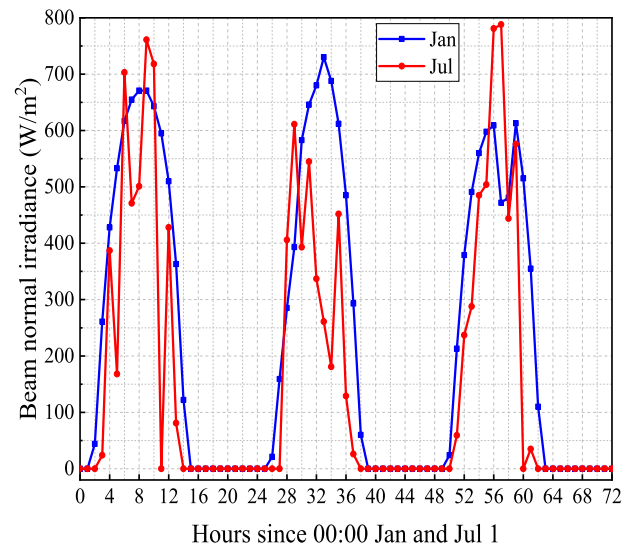


Fig. 11. Thermal power incident on the receiver in the solar field for hot and cold months (MWt).

in co-generation plants due to steam extraction per extracted heat, can be used as the logical indicator for selecting the most optimum points. Table 13 gives the power loss factor of some certain points corresponding to the four possible steam extraction points and six steam return points (see Fig. 7). These results suggest that the minimum value of the power loss factor is 12.8%, which is corresponded to the SP1 and SR2, SR3 points. The present results are significant in at least two major respects: First, minimizing the electricity loss, and second, minimizing the heat cost required for thermal DP.

In the co-generation plant, the leveled energy cost is different since the annual electricity production and thermal utilization of NPP are changed. In order to evaluate the LCOE of ALFRED-based co-generation plant, the new E_{Annual} should be calculated (see Table 6). The LCOH of the co-generation plant depends on the power loss factor of the system and can be obtained by [47]:

$$LCOH_{co-generation} (\text{cent/kW.h}) = LCOE_{NPP} \times \text{Power loss factor} \quad (40)$$

In Fig. 17, the LCOH and LCOE of ALFRED-based co-generation NPP are demonstrated. As can be seen, the minimum LCOH and LCOE can be

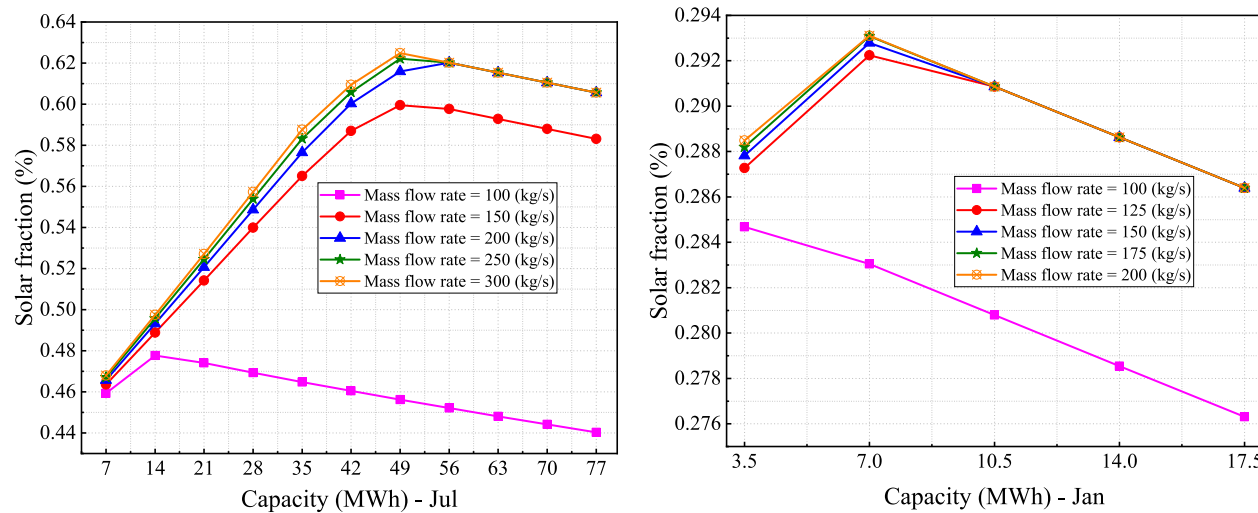


Fig. 12. Solar fraction depending on various maximum HTF mass flow rates and different PCMSS capacities.

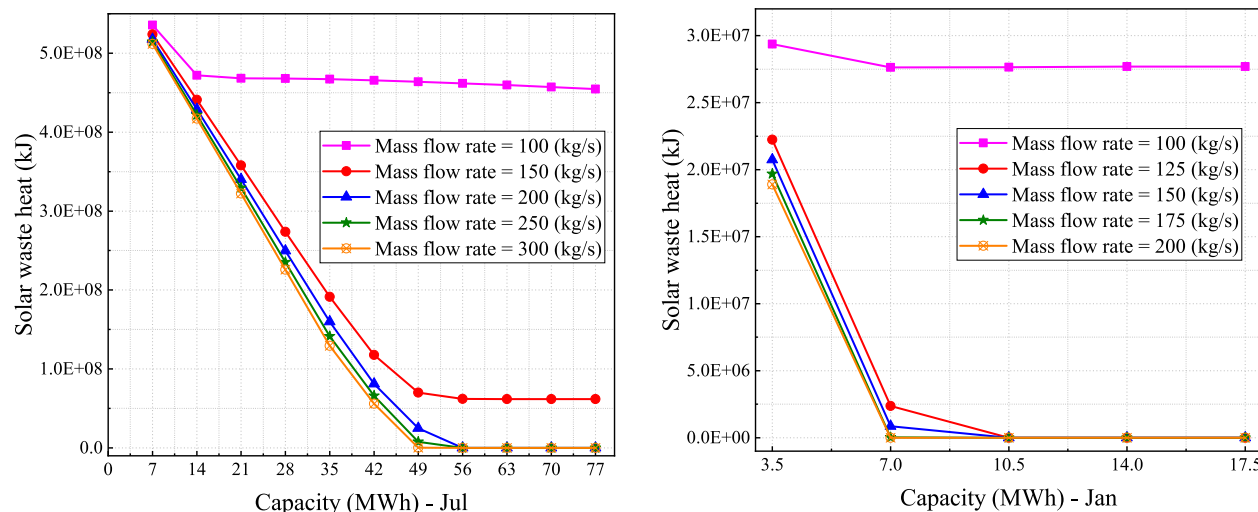


Fig. 13. The solar waste heat versus a continuous range of PCMSS capacity based on various maximum HTF mass flow rates.

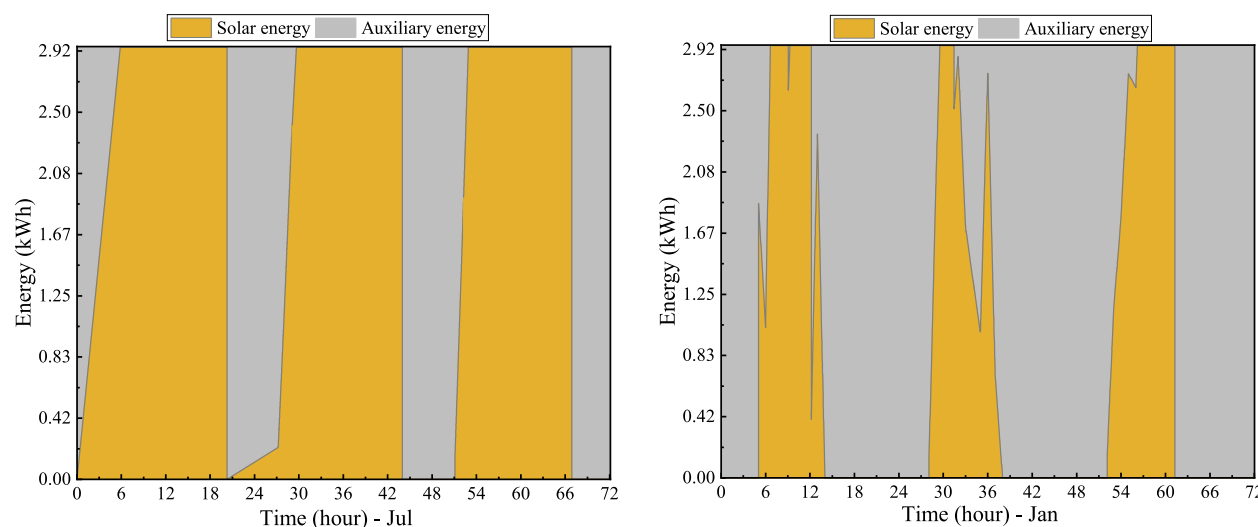


Fig. 14. Consumed solar and auxiliary energy for supplying the required energy of thermal DP.

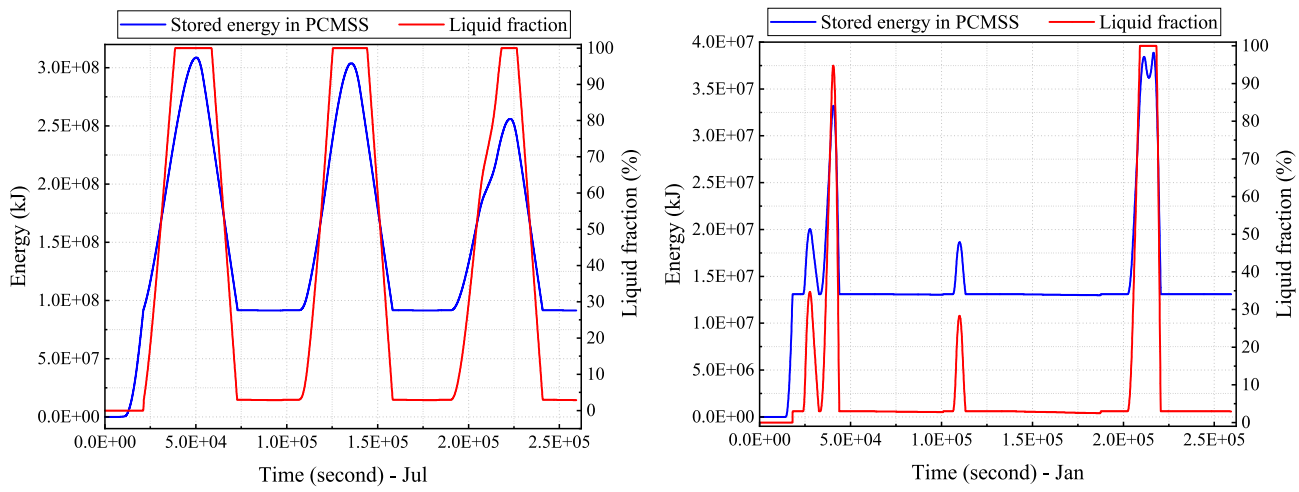


Fig. 15. Stored energy in PCMSS and liquid fraction of PCM.

Table 8

Main input parameters for the economic evaluation of ALFRED-based NPP [42,43,45].

Parameter	Value	Parameter	Value
Construction duration (month)	60	Specific construction cost (\$/kWe)	4903
Lifetime of energy plant (year)	60	Specific operating and maintenance cost (\$/MWhe)	13
Power plant availability (%)	80	Energy plant contingency factor (%)	30
Additional site related construction cost factor (%)	10	α (%)	66
Interest rate (%)	1.5	Discount rate (%)	0.0

Table 9

Main input parameters for the economic evaluation of SF.

Parameter	Value
Solar field cost (\$/m ²)	230
PCM (\$/m ²)	2180
HTF (water) (\$/kg)	0.001
Carbon steel (including shop fabrication, shipping & field fabrication) (\$/kg)	4.4
Insulation (\$/m ²)	206
Cost per unit area of heat exchanger (\$/m ²)	894 [46]
Foundation (\$/m ²)	1199
Other costs (including electrical and instrumentation, Piping, valves, and fittings)	10% of total specific installation costs

Table 10

Comparison of consumed energy and total energy cost of SPP in different months.

Time	Total auxiliary energy (TJ)	Total solar energy (TJ)	$LCOH_{SPP}^{total}$ (cent/kWh)
July	First day	0.345	0.569
	Second day	0.297	0.618
	Third day	0.317	0.598
Jan	First day	0.630	0.285
	Second day	0.677	0.238
	Third day	0.624	0.291

Table 11

The details of the energy costs in thermal DP.

Time		Electricity cost (cent/m ³)	Heat cost (cent/m ³)	Total energy cost (cent/m ³)
July	First day	14.9	30.9	45.7
	Second day	14.9	29.7	44.5
	Third day	14.9	30.2	45.0
	Jan	First day	14.9	38.1
	Second day	14.9	38.9	0.529
	Third day	14.9	37.9	0.538

Table 12

The details of the water cost in the first scenario.

Time		Total water cost of MED plant (cent/m ³)	Total water cost of RO plant (cent/m ³)	Total water cost of the hybrid plant (cent/m ³)
July	First day	976	64	714
	Second day	964	64	711
	Third day	969	64	712
Jan	First day	104.8	64	730
	Second day	105.7	64	732
	Third day	104.6	64	729

achieved by selecting the SPE1 and SR3 points. In this figure, there is a clear trend of increasing electrical power reduction by increasing the power loss factor. Hence, as a final conclusion from Table 14 and Fig. 17, the SP1 and SR2 points can be selected for further calculation.

Table 15 compares the summary of technical results of Standalone ALFRED-based NPP and Co-generation plant for SP1 and SR2 points. It is somewhat surprising that with a small reduction in net output power of co-generation plant (1.4 MWe) due to the steam extraction, not only about 9 MWth less heat is rejected to the condenser, but also the total co-generation plant efficiency increases up to 7% in comparison to stand-alone ALFRED-based NPP. The total cost of treated water in this scheme is about 66 (cent/m³), in which the MED and RO costs are 73 and 64 (cent/m³), respectively.

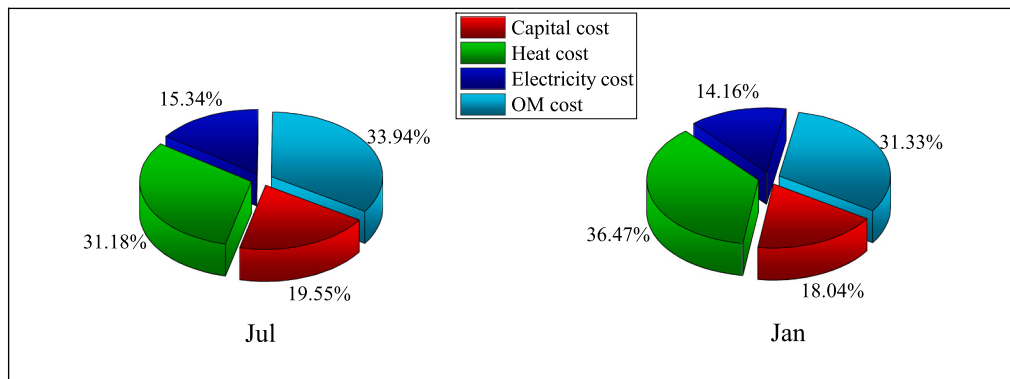


Fig. 16. The portions of different cost components of thermal desalination plant

Table 13
Technical parameters of ALFRED-based NPP calculated by Dymola ALFRED simulator.

Location	Pressure (bar)	Temperature (°C)	Enthalpy (kJ/kg)	Mass flow rate (kg/s)
Before high-pressure turbine	180	480	3206	132
After high-pressure turbine	12.17	189	2667	106
After low-pressure turbine (before condenser)	0.08	40	2248	79
Low pressure pre-heater 1	0.3	69	289	84
Low pressure pre-heater 2	0.96	99	413	89
Low pressure pre-heater 3	2.82	131	553	94
Low pressure pre-heater 4	6.89	164	694	100
Degaerator	14.64	197	840	124
High-pressure pre-heater	39.76	250	1086	142

4.3. Techno-economic evaluation of the third scenario

In the third scenario, the ALFRED-based NPP is integrated into SP as the auxiliary heat source to supply the required energy of thermal DP (see Section 3.3). The amount of extracted steam from NPP directly depends on the average required auxiliary energy in each month. Hence,

by installing a modular PCMSS and storing the received energy from NPP with a constant rate during each month, unpredictable auxiliary energy patterns can be followed. According to the obtained results from Section 4.1, the required amounts of auxiliary energy for hot and cold months are about 38% (1.03 TJ) and 71% (1.95 TJ) of the total required energy, respectively. In a similar way to Section 4.2, the total capacity of the PCMSS integrated into NPP should be optimized. In Fig. 18, the nuclear fractions of auxiliary energy for hot and cold months are presented. As can be seen in this figure, by increasing the amount of extracted energy from NPP, the nuclear fraction increases. The amount of nuclear heat, which is more than the capacity of the PCMSS and should be rejected, is illustrated in Fig. 19. In this figure, there is a clear trend of decreasing nuclear waste heat by increasing the total capacity of the PCMSS for all the possible amounts of heat extracted from NPP. By comparing the reported results in Figs. 18 and 19, it can be concluded that the capacities of 49 and 42 (MWh) and extracted heat of 4 and 7

Table 14
Power loss factor of some certain points corresponding to the four possible steam extraction points and six steam return points (see Fig. 7).

Steam return point	Power lost factor (%)			
	SEP1	SEP2	SEP3	SEP4
SR1	13.1	19.6	25.7	30.8
SR2	12.8	18.8	24.6	29.1
SR3	12.8	18.5	23.9	27.8
SR4	13.1	18.5	23.6	27
SR5	13.5	18.7	23.6	26.7
SR6	14.7	19.4	23.9	26.7

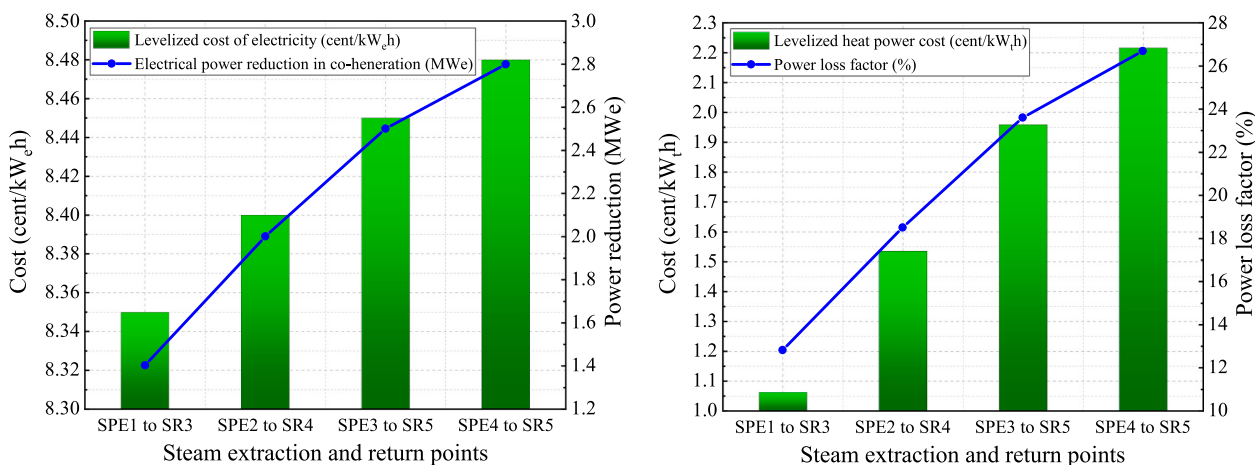


Fig. 17. The variation of leveled cost of heat and electricity, power loss factor, and electrical power reduction of ALFRED-based co-generation.

Table 15

Technical results of Standalone ALFRED-based NPP and Co-generation plant corresponding to SP1 and SR2 points.

Parameter	Standalone ALFRED-based NPP	Co-generation plant	Unit
Gross efficiency	41.5	41.1	%
Total co-generation plant efficiency	41.9	45	%
Heat rate	8.578	8.671	$\frac{\text{kJ}}{\text{kWh}}$
High-pressure turbine output power	67.5	67.5	MWe
Low-pressure turbine output power	67.7	66.3	MWe
Auxiliary loads (such as feedwater pumps)	3.4	3.4	MWe
Net power output	125.9	124.5	MWe
Heat rejected condenser	165	156	MWth
Mass flow rate of low-pressure turbine exhaust	79.2	74.9	$\frac{\text{kg}}{\text{s}}$

(MW) for hot and cold months, respectively, provide a suitable condition for storing the required energy. Regarding Fig. 18, almost 22 and 14% of the total required heat in each month should be supplied by an electrical heater.

The obtained results of the techno-economic evaluation of the third

scenario have been summarized in Table 16. The required heat from NPP for both months can be supplied from SP1 point (see Fig. 7) with various amounts of mass flow rates. The average LCOE in the hot month is a little less than the cold month since the total electricity production during the hot month is more than the cold month.

4.4. General comparison between various scenarios

In this section, the general comparisons for all the possible schemes are carried out. The obtained results are listed in Table 17. The comparison gives the following results:

- 1- The LCOE of scenario 3 is lower than other scenarios, while the LCOH of scenario 2 is significantly less than scenarios 1 and 2.
- 2- From the economic point of view, scenario 2 is the best option due to the lowest water cost.
- 3- In scenario 2, the increase in total co-generation plant efficiency in comparison to standalone alone plant is almost 7% while this number for scenario 3 is not more than 4%.
- 4- If the required heat energy for driving the thermal DP is supplied by natural gas fuel instead of nuclear and solar, the amount of CO₂ produced would be almost 20,000 tons per year.
- 5- The risk of integration of the system with NPP and radioactive emission to the environment in scenario 1 is less than other scenarios

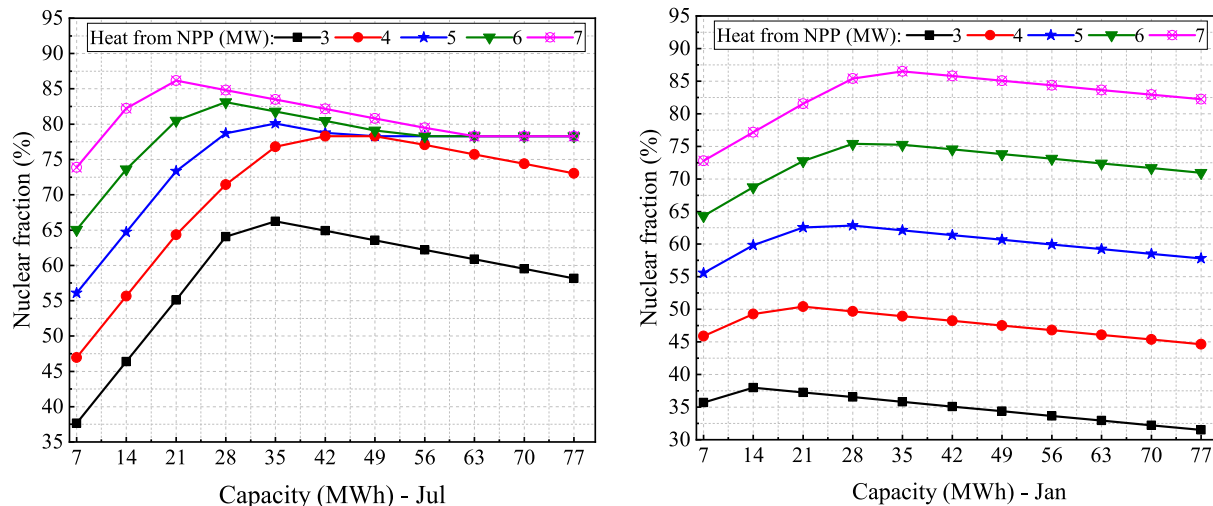


Fig. 18. Nuclear fraction depending on various amounts of extracted heat from NPP and different PCMSS capacities.

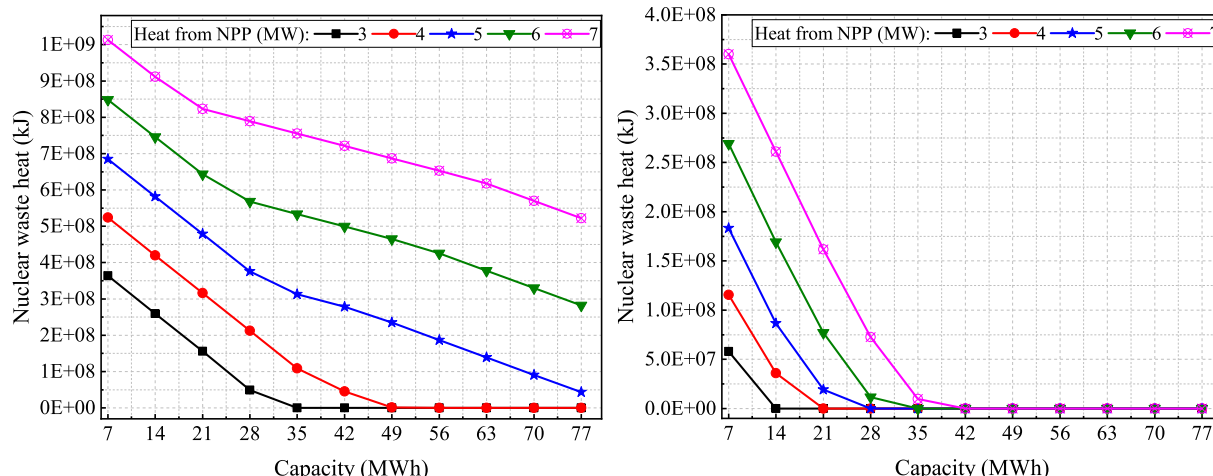


Fig. 19. The nuclear waste heat versus a continuous range of PCMSS capacity based on various amounts of extracted heat from NPP.

Table 16

The results of the techno-economic evaluation of the third scenario.

Parameter	Hot month	Cold month	Unit
Extracted heat from NPP	4	7	MW _{th}
Properties of extracted steam: temperature, pressure, mass flow rate	99, 0.96, 1.9	99, 0.96, 3.2	°C, bar, $\frac{\text{kg}}{\text{s}}$
Power loss factor	12.7	12.8	%
Total co-generation plant efficiency	43.1	44	%
Net power output	125.4	125.12	MWe
Heat Rejected Condenser	161	159	MW _{th}
Number of PCMS modules	7	6	$\times 7$ (MWh)
Contribution of different heat source: nuclear, solar, heater	29.6, 62, 8.38	61.7, 29, 9.23	%
Average LCOE	8.32	8.33	cent/kW _h
Average LCOH of NPP	1.050	1.066	cent/kW _h
Average LCOH of SP	5.46	7.02	cent/kW _h
Total LCOH (average of NPP, solar and heater)	4.39	3.46	cent/kW _h
Water cost produced from RO unit	64.1	64.2	cent/m ³
Water cost produced from MED unit	90.6	85.6	cent/m ³
Total water cost	69.93	68.9	cent/m ³

Table 17

A comprehensive comparison between suggested scenarios.

Parameter	Scenario 1	Scenario 2	Scenario 3
Levelized electrical costs ($\frac{\text{cent}}{\text{kW}_e\text{h}}$)	8.3	8.35	8.325
Levelized heat costs ($\frac{\text{cent}}{\text{kW}_h}$)	6.24	1.062	3.91
Total water cost ($\frac{\text{cent}}{\text{m}^3}$)	72.1	66	69.41
Number of PCMS modules	8	0	13
Factors with positive impacts			
Increase in total co-generation plant efficiency	✗	✓ (high)	✓ (medium)
Utilizing the renewable energy source	✓	✗	✓
Zero CO ₂ emission	✓	✓	✓
Factors with negative impacts			
Reduction in NPP efficiency	✗	✓ (high)	✓ (medium)
Risk of integration with NPP	✓ (low)	✓ (medium)	✓ (medium)
Electricity conversion to heat	✓ (high)	✗	✓ (low)

since in this scheme only the rejected water of NPP's condenser is used as the feedwater of DPs.

- 6- The electricity conversion to heat as the auxiliary energy source is an undesired process. In scenario 3, the amount of this parameter is lower than scenario 1 since the main auxiliary heat source is extracted steam from NPP.

5. Conclusion

In this study, the possibility of using the rejected water from NPP's condenser as the feedwater of DPs was discussed. Despite the fact that using the high-temperature water of the condenser has some positive effects on the overall performance of the desalination system, the main negative impact is increasing the TDS of produced water from RO unit. It was proved that by applying the hybridization factor of 22%, the quality of produced water can attain the standard level for drinking. However, producing 22% of total freshwater through thermal DPs needs a certain amount of heat energy. In line with the net-zero emission goals, the selected heat sources in this work were solar, nuclear, and solar-nuclear hybrid power plants. The main purpose of the current study was to perform a techno-economic assessment of three different scenarios

based on the mentioned heat sources.

According to the obtained results for scenario 1, the modularity in PCMS can increase the capability of energy-storing in both hot and cold months. The findings from this study express that selecting the 300 and 150 (kg/s) of maximum HTF mass flow rates (and higher) at 49 and 7 MWh capacities for hot and cold months respectively, can provide the minimum solar waste heat and maximum solar fraction. In the second scenario, it was shown that with a small reduction in net output power of co-generation plant (1.4 MWe) due to the steam extraction, not only about 9 MW_{th} less heat is rejected to the condenser, but also the thermal utilization of the system increases up to 7% in comparison to standalone ALFRED-based NPP. In scenario 3, the number and capacity of PCMS modules integrated into NPP were investigated. The results in this scheme show that the contribution of NPP in supplying the total required heat varies from 30 to 61% during the hot and cold months, respectively. The average water cost in scenario 2 is almost 66 ($\frac{\text{cent}}{\text{m}^3}$), which almost 8.5 and 5% is less than scenarios 1 and 3. Hence, it can be concluded that from the economic point of view, scenario 2 is more appropriate in comparison to other schemes. Although the water cost of scenario 3 is higher than scenario 2, the existence of the renewable source in this scheme can be associated with some benefits such as load following or peak shaving. However, the analysis of these factors is beyond the scope of this study can be considered as further works. The obtained data are broadly consistent with the major trends of economic evaluations, which have been conducted in other researches.

The key strength of this study was comparing several possible energy sources for driving the thermal DP to increase the quality of produced water of RO unit. However, the combination of solar and SMR-based NPP as a hybrid system is a promising technology, which can be used for many other applications. In spite of the fact that the general technical analysis of hybrid energy sources has been considered in this paper, more researches on thermodynamic aspects such as designing new types of PCMS or safety analysis of nuclear desalination are still necessary before designing large-scale hybrid co-generation plants. Based on the promising findings presented in this paper, work on the remaining issues is continuing.

Funding

This work was supported by RFBR according to the research project No. 20-38-90048.

Declaration of competing interest

The authors declare that they have no known competing financial interests or personal relationships that could have appeared to influence the work reported in this paper.

References

- [1] S. Tsani, P. Koundouri, E. Akinsete, Resource management and sustainable development: a review of the European water policies in accordance with the United Nations' sustainable development goals, *Environ. Sci. Pol.* 114 (2020) 570–579.
- [2] P. Guo, T. Li, Y. Wang, J. Li, Energy and exergy analysis of a spray-evaporation multi-effect distillation desalination system, *Desalination* 500 (2021), 114890.
- [3] E. Rosales-Asensio, A.-E. Rosales, A. Colmenar-Santos, Surrogate optimization of coupled energy sources in a desalination microgrid based on solar PV and wind energy, *Desalination* 500 (2021), 114882, <https://doi.org/10.1016/j.desal.2020.114882>.
- [4] M.T. Mito, X. Ma, H. Albuflasa, P.A. Davies, Reverse osmosis (RO) membrane desalination driven by wind and solar photovoltaic (PV) energy: state of the art and challenges for large-scale implementation, *Renew. Sustain. Energy Rev.* 112 (2019) 669–685.
- [5] K. Sadeghi, S.H. Ghazaei, E. Sokolova, E. Fedorovich, A. Shirani, Comprehensive techno-economic analysis of integrated nuclear power plant equipped with various hybrid desalination systems, *Desalination* 493 (2020), 114623.
- [6] K. Elsaid, M. Kamil, E.T. Sayed, M.A. Abdelkareem, T. Wilberforce, A. Olabi, Environmental impact of desalination technologies: a review, *Sci. Total Environ.* 748 (2020), 141528.

- [7] N.A. Ahmad, P.S. Goh, L.T. Yogarathinam, A.K. Zulhairun, A.F. Ismail, Current advances in membrane technologies for produced water desalination, *Desalination* 493 (2020), 114643.
- [8] S. Lin, H. Zhao, L. Zhu, T. He, S. Chen, C. Gao, L. Zhang, Seawater desalination technology and engineering in China: a review, *Desalination* 498 (2021), 114728.
- [9] A. Al-Othman, N.N. Darwish, M. Qasim, M. Tawalbeh, N.A. Darwish, N. Hilal, Nuclear desalination: a state-of-the-art review, *Desalination* 457 (2019) 39–61.
- [10] Y. Zheng, R.A. Caceres Gonzalez, K.B. Hatzell, M.C. Hatzell, Large-scale solar-thermal desalination, *Joule* 5 (8) (2021) 1971–1986.
- [11] F.J. Jamshidian, S. Gorjian, M. Shafieefar, Techno-economic assessment of a hybrid RO-MED desalination plant integrated with a solar CHP system, *Energy Convers. Manag.* 251 (2022), 114985.
- [12] V.G. Gude, Energy consumption and recovery in reverse osmosis, *Desalin. Water Treat.* 36 (1–3) (2011) 239–260.
- [13] H.T. Do Thi, T. Pasztor, D. Fozer, F. Manenti, A.J. Toth, Comparison of desalination technologies using renewable energy sources with life cycle, PESTLE, and multi-criteria decision analyses, *Water* 13 (21) (2021) 3023.
- [14] A.G. Olabi, K. Elsaied, M.K.H. Rabaia, A.A. Askalany, M.A. Abdelkareem, Waste heat-driven desalination systems: perspective, *Energy* 209 (2020), 118373.
- [15] M. Gong, M. Peng, H. Zhu, Research of parameter distributing simulation and modeling for the condenser in nuclear power plant, *Ann. Nucl. Energy* 133 (2019) 313–326.
- [16] S. Talebi, N. Norouzi, Entropy and exergy analysis and optimization of the VVER nuclear power plant with a capacity of 1000 MW using the firefly optimization algorithm, *Nucl. Eng. Technol.* 52 (12) (2020) 2928–2938.
- [17] C.P. Koutsou, E. Kritikos, A.J. Karabelas, M. Kostoglou, Analysis of temperature effects on the specific energy consumption in reverse osmosis desalination processes, *Desalination* 476 (2020), 114213.
- [18] I.W. Son, Y.H. Jeong, Y.J. Choi, J.I. Lee, Feasibility study of solar-nuclear hybrid system for distributed power source, *Energy Convers. Manag.* 230 (2021), 113808.
- [19] S.H. Ghazaei, K. Sadeghi, E. Sokolova, E. Fedorovich, A. Shirani, Comparative analysis of hybrid desalination technologies powered by SMR, *Energies* 13 (19) (2020).
- [20] S.H. Ghazaei, K. Sadeghi, E. Sokolova, E. Fedorovich, A. Shirani, Nuclear desalination in Iran, current status and perspectives, *E3S Web Conf.* 140 (2019).
- [21] K. Sadeghi, S.H. Ghazaei, E.D. Fedorovich, E.A. Sokolova, A.S. Shirani, Economic assessment of the possible desalination processes for the first unit of Bushehr nuclear power plant, *Therm. Eng.* 67 (5) (2020) 271–281.
- [22] K. Sadeghi, S.H. Ghazaei, E. Sokolova, E. Fedorovich, A. Shirani, Thermo-economic assessment of the possible desalination processes for the second block of Bushehr nuclear power plant, *E3S Web Conf.* 140 (2019).
- [23] I. Al-Mutaz, M. Ghunaimi, Performance of Reverse Osmosis Units at High Temperatures, 2001.
- [24] S. International Programme on Chemical <collab>O. World Health, Guidelines for drinking-water quality, in: *Health Criteria and Other Supporting Information vol. 2*, World Health Organization, Geneva, 1996.
- [25] K. Velmurugan, S. Kumarasamy, T. Wongwuttanasatian, V. Seithantanabutara, Review of PCM types and suggestions for an applicable cascaded PCM for passive PV module cooling under tropical climate conditions, *J. Clean. Prod.* 293 (2021), 126065, <https://doi.org/10.1016/j.jclepro.2021.126065>.
- [26] L. Guzman, A. Henao, R. Vasquez, Simulation and optimization of a parabolic trough solar power plant in the city of Barranquilla by using system advisor model (SAM), *Energy Procedia* 57 (2014) 497–506.
- [27] A. Dobos, T. Neises, M. Wagner, Advances in CSP simulation technology in the system advisor model, *Energy Procedia* 49 (2014) 2482–2489.
- [28] J.F. Belmonte, P. Egúfa, A.E. Molina, J.A. Almendros-Ibáñez, R. Salgado, A simplified method for modeling the thermal performance of storage tanks containing PCMs, *Appl. Therm. Eng.* 95 (2016) 394–410.
- [29] P. Gilman, N. Blair, M. Mehos, C. Christensen, S. Janzou, C. Cameron, *Solar Advisor Model User Guide for Version 2.0*, United States, 2008.
- [30] Desalination Economic Evaluation Program (DEEP), INTERNATIONAL ATOMIC ENERGY AGENCY, Vienna, 2000.
- [31] M. Methnani, DEEP: a tool for evaluation co-generated power and desalination strategies, *Desalination* 166 (2004) 11–15.
- [32] K.C. Kavvadias, I. Khamis, The IAEA DEEP desalination economic model: a critical review, *Desalination* 257 (1) (2010) 150–157.
- [33] Q. Wang, G. Pei, H. Yang, Techno-economic assessment of performance-enhanced parabolic trough receiver in concentrated solar power plants, *Renew. Energy* 167 (2021) 629–643.
- [34] K. Attonaty, J. Povreau, A. Deydier, J. Oriol, P. Stouffs, Thermodynamic and economic evaluation of an innovative electricity storage system based on thermal energy storage, *Renew. Energy* 150 (2020) 1030–1036.
- [35] S. Mazzoni, J.Y. Sze, B. Nastasi, S. Ooi, U. Desideri, A. Romagnoli, A techno-economic assessment on the adoption of latent heat thermal energy storage systems for district cooling optimal dispatch & operations, *Appl. Energy* 289 (2021), 116646.
- [36] M. Abbas, Z. Belgroun, H. Aburidah, N.K. Merzouk, Assessment of a solar parabolic trough power plant for electricity generation under Mediterranean and arid climate conditions in Algeria, *Energy Procedia* 42 (2013) 93–102.
- [37] E. Spoletilini, Levelized cost of energy (lcoe) analysis of a low temperature PCM thermal storage combined with a micro-CHP in an apartment block, *Energy Procedia* 126 (2017) 437–444.
- [38] R. Ponciroli, A. Bigoni, A. Cammi, S. Lorenzi, L. Luzzi, Object-oriented modelling and simulation for the ALFRED dynamics, *Prog. Nucl. Energy* 71 (2014) 15–29.
- [39] R. Ponciroli, A. Cammi, S. Lorenzi, L. Luzzi, A preliminary approach to the ALFRED reactor control strategy, *Prog. Nucl. Energy* 73 (2014) 113–128.
- [40] R. Ponciroli, A. Cammi, S. Lorenzi, L. Luzzi, Petri-net based modelling approach for ALFRED reactor operation and control system design, *Prog. Nucl. Energy* 87 (2016) 54–66.
- [41] R. Ponciroli, A. Cammi, A. Della Bona, S. Lorenzi, L. Luzzi, Development of the ALFRED reactor full power mode control system, *Prog. Nucl. Energy* 85 (2015) 428–440.
- [42] S. Boarin, M.E. Ricotti, An evaluation of SMR economic attractiveness, *Sci. Technol. Nucl. Install.* 2014 (2014), 803698.
- [43] F. Aydogan, G. Black, M.A. Taylor Black, D. Solan, Quantitative and qualitative comparison of light water and advanced small modular reactors, *J. Nucl. Eng. Radiat. Sci.* 1 (4) (2015).
- [44] G. Cau, D. Cocco, Comparison of medium-size concentrating solar power plants based on parabolic trough and linear fresnel collectors, *Energy Procedia* 45 (2014) 101–110.
- [45] A. Alemberti, Lead Cooled Fast Reactors, Reference Module in Earth Systems and Environmental Sciences, Elsevier, 2020.
- [46] A.-S. Hamed, S. Sadeghzadeh, Conceptual design of a 5 MW OTEC power plant in the Oman Sea, *J. Mar. Eng. Technol.* 16 (2) (2017) 94–102.
- [47] Nuclear–Renewable Hybrid Energy Systems for Decarbonized Energy Production and Cogeneration, INTERNATIONAL ATOMIC ENERGY AGENCY, Vienna, 2019.